Study of the N-soliton solution for the (2 + 1)-dimensional generalized Bogoyavlensky-Konopelchenko equation

Abstract

This paper presents a systematic investigation of the N-soliton solutions for the (2+1) -dimensional generalized Bogoyavlensky-Konopelchenko equation. By employing the Hirota bilinear method, we have rigorously derived the analytical expressions of the N-soliton solutions. By virtue of the Maple software, various three-dimensional structural patterns and the corresponding density distribution plots are generated. Furthermore, the interaction evolution behaviors of soliton solutions are also exhibited graphically by selecting different time values, providing visual illustrations of the dynamical process of soliton solutions. It is demonstrated well that the studied equation has various special interaction patterns between different soliton types, such as interaction solutions between lump and line solitons, as well as those between periodic and line solitons. Numerical simulations indicated that all these interactions exhibit the characteristics of elastic collisions. This study provides some inherent insights for better understanding the soliton behaviors occurred in integrable system fields including nonlinear physics, fluid mechanics, optical fiber communication and so on.
Keywords: (2+1)-Dimensional generalized Bogoyavlensky–Konopelchenko equation, Line Soliton, Kink Soliton, Periodic Soliton, Lump Soliton

1 Introduction

The theory of solitons is an extremely important branch in mathematics and physics, connecting multiple fields such as fluid mechanics, oceanography, particle physics and even biology. Its core research object is the solitary wave, also known as the soliton. A solitary wave is a particular type of exact solution to certain nonlinear partial differential equations. Therefore, it is of great significance to study the exact solutions of nonlinear systems. So far, there are various exact solution research methods, including inverse scattering transformation (Gardner et al., 1976; Ablowitz et al., 1974; Ma & Zhu, 2023; Chen & Yan, 2022; Shepelsky & Zielinski, 2017; Bilman & Miller, 2019), Darboux transformation (Wu & Gao, 2023; Tchokouansi et al.,2016; Ling, et al., 2015; Wang & Wei, 2022; Xia et al., 2016; Geng & Tam, 1999), Riemann-Hilbert method (Li et al., 2022; Fokas & Kapaev, 2000; Zuo & Guo, 2023; Ai & Xu, 2019), perturbation methods (Gorshkov & Ostrovsky, 1981), Bäcklund transformation (Hirota, 1974; Lü et al., 2007; Lu et al., 2015; Wahlquist & Estabrook, 1973; Hirota & Satsuma, 1977), Hirota bilinear method (Ma et al., 2012; An & Guo, 2023; Gao et al., 2016; Pashaev & Tanoğlu, 2005; Li et al., 2023; Mandal et al., 2023; Hietarinta, 1987; Hietarinta, 1996; Saifullah et al., 2022; Hua et al., 2019; Mabrouk & Rashed, 2019; Ma, 2022; Biswas et al., 2023) and many other effective approaches (Clarkson & Kruskal, 1989; Ludlow et al., 1999; Lou et al., 2000; Ma, 2004; Freeman & Nimmo, 1983; Ünal, 2010; Hirota, 1989).

Among the methods of solving nonlinear systems, the Hirota bilinear method is highly favored for its simple and straightforward. The essence of the Hirota bilinear method lies in transforming nonlinear equations into bilinear equations through variable substitution and then solve them using specific forms of solutions such as logarithmic functions. This method is frequently used to construct soliton solutions. Fang et al. (Fang & Wang,2018) obtained the interaction solutions of the dimensionally reduced equations in (2+1)-dimensions achieved via Hirota bilinear method. Zuo et al. (Zuo & Zhang,2011) employed Hirota bilinear method to establish the complete integrability of two systems: the coupled Burgers equations and the higher-order Boussinesq-Burgers equations. Their work

also led to the derivation of different type of solutions, including multi-kink and multi-singular-kink soliton solutions. Wang et al. (Wang, 2023) used the Hirota bilinear method to study a (2+1)-dimensional inhomogeneous PT-symmetric coupled nonlinear Schrödinger equation, enabling the derivation of its soliton solutions. Han et al. (Han et al., 2025) pioneered a bilinear neural network method grounded in the generalized bilinear transformation to study the (3+1)-dimensional Hirota–Satsuma–Ito equation, utilizing Maple software for symbolic computation, the research revealed the equation's rich solution structures, including periodic solution, and complex wave interaction solution. Over the past few years, the Hirota bilinear method serves as a powerful tool for analyzing rational solutions across a wide range of equations, and common types of solitons include breather solutions and lump solutions. Johansson et al. (Johansson & Aubry, 1997) undertook a comprehensive study focusing on the stability properties of multiple breather solutions for the standard nonlinear Schrödinger equation. Lv et al. (Lv et al., 2023) examined a (2+1)-dimensional variable-coefficient equation modeling nonlinear wave dynamics in compressible hyperelastic plates. By utilizing symmetric transformations and the Hirota bilinear form, they formulated solutions for both breather waves and rogue waves. Liu et al. (Liu et al., 2019) utilized the bilinear method and the test function approach to systematically solve the (2+1)-dimensional generalized HSI equation. They successfully derived its multi-soliton solutions and constructed complex exact solutions representing the interactions between various types of localized waves and solitons.

The (2+1)-dimensional Bogoyavlensky-Konopelchenko equation is a typical model for studying the dynamics of nonlinear waves. Faisal et al. (Faisal & Maqbool, 2015) investigated a variety of exact soliton solutions for the equation using the exponential function expansion method and the modified Kudryashov method. Ray et al. (Saha, 2017) derived the conservation laws for this equation using Lie group analysis method. Yoku et al. (Yokuş et al., 2024) proposed a new method for studying variable coefficients (2+1)-dimensional Bogoyavlensky-Konopelchenko equation and obtained it's traveling wave solutions. Triki et al. (Triki et al., 2014) used Ansatz approach and obtained the shock wave solution of this equation. Inspired by the aforementioned studies, this paper introduces the following (2+1)-dimensional generalized Bogoyavlensky-Konopelchenko (gBK) equation.

$$\mathrm{gBK}(u,v) := u_t + \gamma_1(6uu_x + u_{xxx}) + \gamma_2(u_{xxy} + 3uu_y + 3u_xv_y) + \gamma_3u_x + \gamma_4u_y + \gamma_5v_{yy} = 0, \tag{1}$$

where $u = v_x$, and $\gamma_1, \gamma_2, \gamma_3, \gamma_4, \gamma_5$ are constant coefficients. This equation can be rewritten as follows equivalent form

$$v_{tx} + \gamma_1(6v_xv_{xx} + v_{xxxx}) + \gamma_2(v_{xxxy} + 3v_xv_{xy} + 3v_{xx}v_y) + \gamma_3v_{xx} + \gamma_4v_{xy} + \gamma_5v_{yy} = 0, \tag{2}$$

the functions u and v are related to the variables x, y and t. A large number of literature have conducted extensive research on the soliton solution types of this equation. Akram et al. (Akram et al. 2023) investigated the equation and obtained many kinds of solitary wave solution. Chen et al. (Chen & Ma, 2018) studied the equation and obtained explicit lump solution. Mnanfian et al. (Manafian et al., 2020) studied many kinds of wave solutions of the equation by applying the bilinear method. Razzaq et al. (Razzaq & Zafar, 2025) investigated the equation and obtained the lump-kink and rogue wave solutions using the bilinear method. Moreover, they also studied the integrability of the given equation. As far as we know, soliton interaction phenomena regarding this equation have not been thoroughly investigated. In this paper, we will focus on the study of the N soliton solution of the (2+1) dimensional gBK equation via the application of the Hirota bilinear method. Furthermore, various interaction characteristics of soliton solution will be discussed. By using Maple software, the three - dimensional plots and energy distribution plots of these interaction solutions are also shown.

This paper is structured as follows: In section 2, the derivation of the analytical expressions for the N-soliton solutions is accomplished through the bilinear method. Next, by imposing constraints on the parameters from two-soliton to four-soliton solutions, various localized interaction solutions are constructed. These solutions are demonstrated with the aid of diagrams. Lastly, some summarizing remarks are provided in section 3.

2 The N-soliton solution of the (2+1)-dimensional gBK equation

In this section the following form is employed, given as

$$u = 2(\ln f)_{xx},\ v = 2(\ln f)_x, \tag{3}$$

and Eq. (3) is substituted into Eq. (1), we can obtain

$$\begin{aligned} gBK(f) = 2\big[&f_{tx}f - f_t f_x + \gamma_1(f_{xxxx}f - 4f_{xxx}f_x + 3f_{xx}^2) \\ &+ \gamma_2(f_{xxxy}f - f_{xxx}f_y - 3f_{xxy}f_x + 3f_{xx}f_{xy}) \\ &+ \gamma_3(f_{xx}f - f_x^2) + \gamma_4(f_{xy}f - f_x f_y) + \gamma_5(f_{yy}f - f_y^2) \\ &= 0. \end{aligned} \tag{4}$$

Meanwhile, based on the definition of the D-operator (Grammaticos et al., 1994)

$$D_x^m D_y^n D_t^p (a \cdot b) = (\partial_x - \partial_{x'})^m (\partial_y - \partial_{y'})^n (\partial_t - \partial_{t'})^p a(x,y,t) b(x',y',t')\big|_{x=x',y=y',t=t'}, \tag{5}$$

we obtain the bilinear form of the gBK equation, written as follows

$$(D_t D_x + \gamma_1 D_x^4 + \gamma_2 D_x^3 D_y + \gamma_3 D_x^2 + \gamma_4 D_x D_y + \gamma_5 D_y^2) f \cdot f = 0, \tag{6}$$

The expressions for the function f are derived through Hirota's bilinear method as follows:

$$\begin{aligned} f = 1 + \sum_{i=1}^{N} \exp(\xi_i) + \sum_{i<j}^{N} A_{ij} \exp(\xi_i + \xi_j) + \sum_{i<j<p}^{N} A_{ij}A_{ip}A_{jp} \exp(\xi_i + \xi_j + \xi_p) \\ + \cdots + \left(\prod_{i<j} A_{ij}\right) \exp\left\{\sum_{i=1}^{N} \xi_i\right\}, \end{aligned} \tag{7}$$

with

$$\begin{aligned} \xi_i &= k_i x + s_i y + w_i t - \xi_{0i} \\ w_i k_i &+ \gamma_1 k_i^4 + \gamma_2 k_i^3 s_i + \gamma_3 k_i^2 + \gamma_4 k_i s_i + \gamma_5 s_i^2 = 0 \\ A_{ij} &= -\frac{M_{ij}}{N_{ij}} \\ M_{ij} =&(w_i - w_j) \cdot (k_i - k_j) + \gamma_1 \cdot (k_i - k_j)^4 + \gamma_2 \cdot (k_i - k_j)^3 \cdot (s_i - s_j) \\ &+ \gamma_3 \cdot (k_i - k_j)^2 + \gamma_4 \cdot (k_i - k_j) \cdot (s_i - s_j) + \gamma_5 \cdot (s_i - s_j)^2 \\ N_{ij} =&(w_i + w_j) \cdot (k_i + k_j) + \gamma_1 \cdot (k_i + k_j)^4 + \gamma_2 \cdot (k_i + k_j)^3 \cdot (s_i + s_j) \\ &+ \gamma_3 \cdot (k_i + k_j)^2 + \gamma_4 \cdot (k_i + k_j) \cdot (s_i + s_j) + \gamma_5 \cdot (s_i + s_j)^2, \end{aligned}$$

where $i, j = 1, 2, \ldots N$. Parameters k_i, s_i and ξ_{0i} are all real parameters, corresponding respectively to the amplitudes and phase characteristics of the soliton.

2.1 One-soliton solution

When $N = 1$, we can obtain the following formula using Eq. (7)

$$f = 1 + \exp(\xi_1). \tag{8}$$

Using Eq. (3) and Eq. (8) directly yields the one-soliton solution of Eq. (1)

$$u = \frac{k_1^2}{2} \mathrm{sech}^2(\frac{1}{2}\xi_1), \tag{9}$$

$$v = \frac{2k_1 \exp(\xi_1)}{1 + \exp(\xi_1)}, \tag{10}$$

where $\xi_1 = k_1 x + s_1 y + w_1 t - \xi_{01}$. Through Eqs. (9) - (10), it is observed that the sign of component u is always positive, while that of v depends entirely on parameter k_1. When we take $k_1 = 6$ and $s_1 = 3$, v also becomes positive. Furthermore, the other parameters are set to $\gamma_1 = 2$, $\gamma_2 = 2$, $\gamma_3 = 1$, $\gamma_4 = 1$, $\gamma_5 = 1$, $\xi_{01} = 0$. The one-soliton solution of Eq. (1) is derived at time $t = 0$, whose profiles are displayed in Fig. 1. It can be found that u exhibits a bell-shaped one soliton while v demonstrates the characteristics of a one-kink soliton. As can be seen from Eqs. (9) - (10), the amplitude of u is $\frac{k_1^2}{2}$, and the amplitude of v is $2k_1$. Their envelope velocities are the same, and both equal to $v_u = v_v = \frac{|w_1|}{\sqrt{k_1^2 + s_1^2}}$.

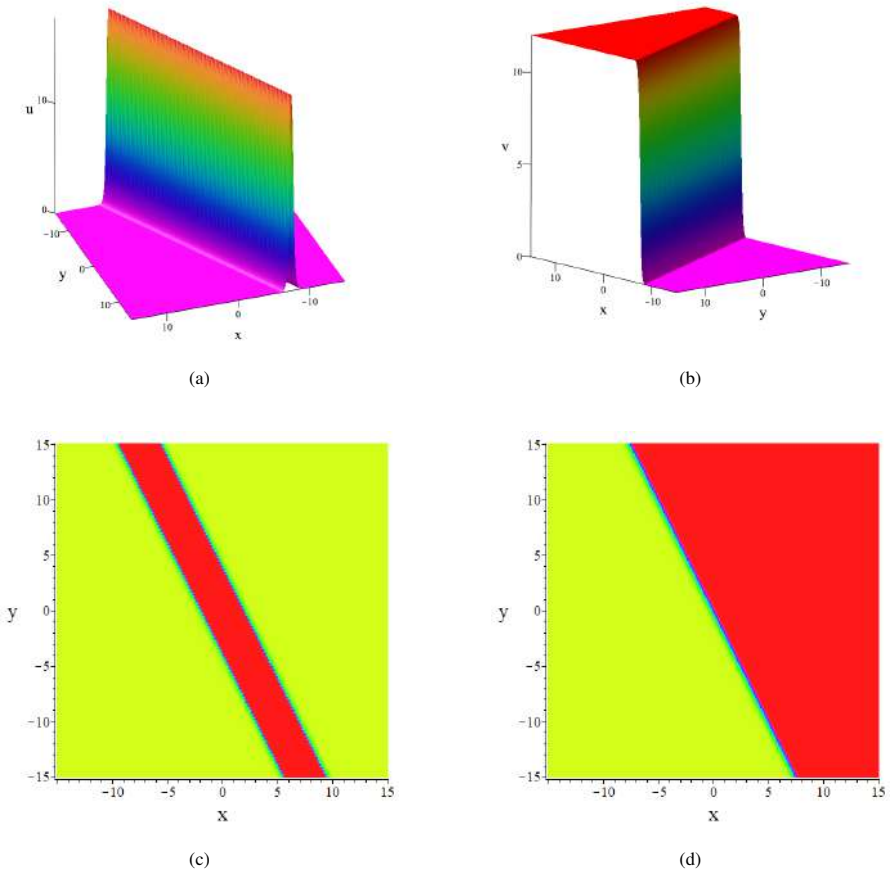

Fig. 1 The one-soliton solution of Eq. (1) at $t = 0$ when the parameters are chosen as follows: $k_1 = 6, s_1 = 3, \xi_{01} = 0, \gamma_1 = 2, \gamma_2 = 2, \gamma_3 = 1, \gamma_4 = 1, \gamma_5 = 1$. (a) 3D structure of u; (b) 3D structure of v; (c) 2D density plot of u; (d) 2D density plot of v

2.2 Two soliton solutions

We set $N = 2$, by virtue of Eq. (7) we can obtain

$$f = 1 + \exp(\xi_1) + \exp(\xi_2) + A_{12}\exp(\xi_1 + \xi_2). \tag{11}$$

By using Eq. (11) and Eq. (3), this yields the two-soliton solutions to Eq. (1), written as follows

$$u = 2 \cdot \left[\frac{k_1 e^{\xi_1} + k_2 e^{\xi_2} + A_{12}(k_1 + k_2) e^{\xi_1+\xi_2}}{1 + e^{\xi_1} + e^{\xi_2} + A_{12} e^{\xi_1+\xi_2}} - \left(\frac{k_1 e^{\xi_1} + k_2 e^{\xi_2} + A_{12}(k_1 + k_2) e^{\xi_1+\xi_2}}{1 + e^{\xi_1} + e^{\xi_2} + A_{12} e^{\xi_1+\xi_2}} \right)^2 \right], \tag{12}$$

$$v = 2 \cdot \frac{k_1 \exp(\xi_1) + k_2 \exp(\xi_2) + A_{12}(k_1 + k_2)\exp(\xi_1 + \xi_2)}{1 + \exp(\xi_1) + \exp(\xi_2) + A_{12}\exp(\xi_1 + \xi_2)}. \tag{13}$$

For different choices of parameters, we can obtain the following four cases of the two-soliton solutions.

2.2.1 The bell-shaped and kink solitons

Firstly, we consider that all parameters take real values in this subsection, and we set $k_1 = 4$, $s_1 = 2$, $k_2 = 1$, $s_2 = 3$, $\xi_{01} = \xi_{02} = 0$, $\gamma_1 = 2$, $\gamma_2 = 2$, $\gamma_3 = 2$, $\gamma_4 = 2$, $\gamma_5 = 2$. By virtue of Maple software, the two solition pattern is shown in Fig. 2. The two bell-shaped soliton solutions of u are shown in Figs. 2a and 2c, respectively, while Figs. 2b and 2d correspond to the soliton v.

2.2.2 The period and kink period solitons

For the Eq. (11), we set the following parameter relationship: $k_1 = k_2 = d_1$, $s_1 = s_{2*} = m_1 + i\delta_1$, $\xi_{01} = \xi_{02} = 0$($i^2 = -1$), and then we have

$$f = 1 + A_{12}\exp(2\alpha_1) + 2\exp(\alpha_1)\cos(\delta_1 y + \psi_1 t), \tag{14}$$

with

$$A_{12} = \frac{\gamma_5\delta^2}{3d_1^4\gamma_1 + 3d_1^3 m_l\gamma_2 + \delta^2\gamma_5},$$

$$\alpha_1 = d_1 x + m_1 y - (d_1^3\gamma_1 + d_1^2 m_1\gamma_2 + d_1\gamma_3 + m_1\gamma_4 + \frac{m_1^3\gamma_5 - \gamma_5\delta_1^2}{d_1})t,$$

$$\psi_1 = -(d_1^2\gamma_2\delta_1 + \delta_1\gamma_4 + \frac{2m_1\delta_1\gamma_5}{d_1}). \tag{15}$$

Specifically, we take $d_1 = \frac{3}{4}$, $m_1 = 0$, $\delta_1 = \frac{3}{2}$, $\gamma_1 = -1$, $\gamma_2 = -1$, $\gamma_3 = 1$, $\gamma_4 = 1$, $\gamma_5 = 1$. It is noted that s_1 and s_2 are both pure imaginary number for this case. Using Maple software, a y-periodic soliton structure of u and a kink periodic soliton structure of v are obtained, as shown in Fig. 3. Among them, Figs. 3a and 3b represent the corresponding three-dimensional plots of u and v respectivey, while Figs. 3c and 3d depict the corresponding energy distribution plots. Their orientations are all perpendicular to the x-axis.

2.2.3 The (x, y)-period and kink-breather solitons

Similarly, for Eqs. (14)-(15), we impose the condition that the parameter s_1 and s_2 are complex numbers and $d_1 = \frac{2}{3}$, $m_1 = 1$, $\delta_1 = \frac{8}{5}$, $\gamma_1 = -1$, $\gamma_2 = -1$, $\gamma_3 = 1$, $\gamma_4 = 1$, $\gamma_5 = 1$. At $t = 0$, we observe that soliton u evolves into a periodic soliton distributed along the (x, y) direction. Figs. 4a and 4c correspond to its three-dimensional plot and density plot, respectively. While soliton v transforms into a kink-breather soliton, displayed in Figs. 4b and 4d. Their configurations maintain unchanged throughout the propagation process.

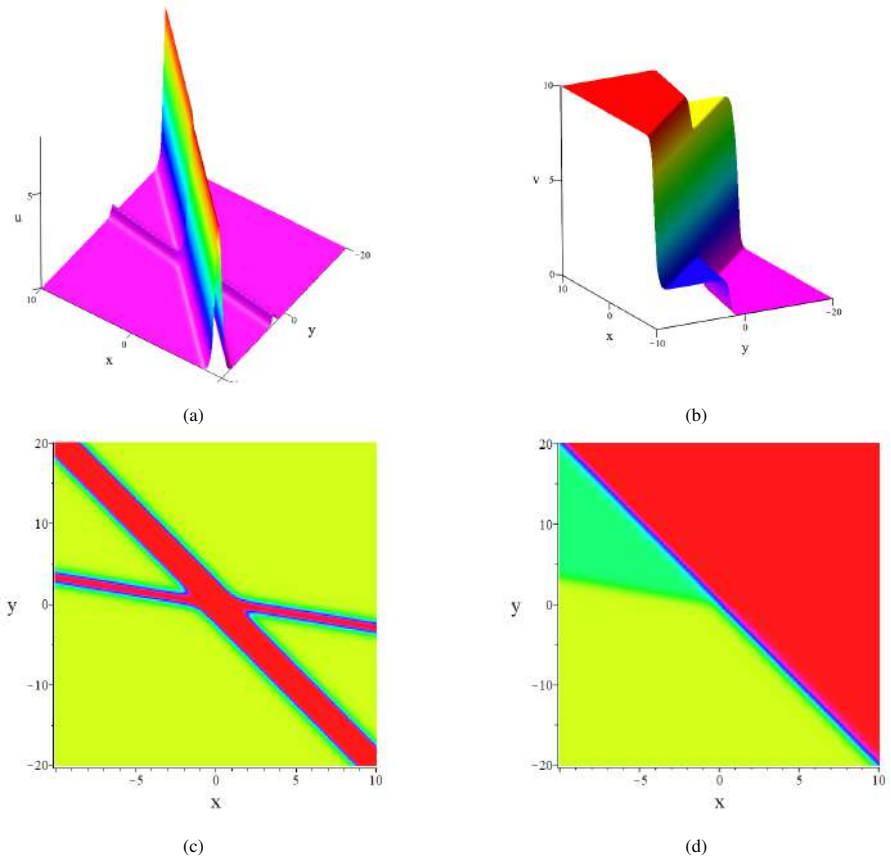

Fig. 2 Two-soliton solutions of Eq. (1) at $t = 0$ when the parameters are chosen as follows: $k_1 = 4$, $s_1 = 2$, $k_2 = 1$, $s_2 = 3$, $\xi_{01} = \xi_{02} = 0$, $\gamma_1 = 2$, $\gamma_2 = 2$, $\gamma_3 = 2$, $\gamma_4 = 2$, $\gamma_5 = 2$. (a) 3D structure of u; (b) 3D structure of v; (c) 2D density plot of u; (d) 2D density plot of v

2.2.4 The lump soliton

In Eq. (14), we adopt the following relationships: $s_1 = l_1 k_1$, $s_2 = l_2 k_2$, $l_1 = l_2^* = 1 + i$. When the parameters k_1, k_2 are taken to be very small, it is found that the two-soliton solutions u and v degenerate into lump soliton. Herein, by substituting specific parameter values $k_1 = 0.01$, $k_2 = 0.01$, $s_1 = 0.01 + 0.01i$, $s_2 = 0.01 - 0.01i$, $\xi_{01} = \xi_{02} = i\pi$, $\gamma_1 = -1$, $\gamma_2 = -1$, $\gamma_3 = 1$, $\gamma_4 = 1$, $\gamma_5 = 1$, we obtain the three-dimensional patterns and density plots of the soliton

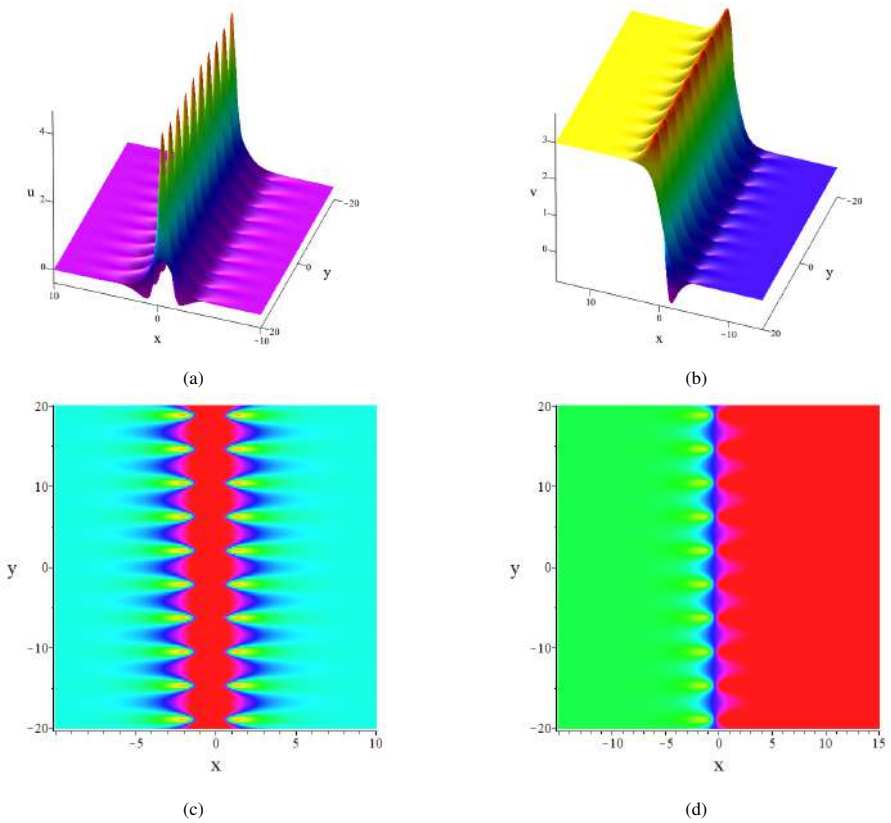

Fig. 3 The y-periodic soliton and kink periodic soliton at $t = 0$ when the parameters are chosen as follows: $s_1 = s_2 = \frac{3}{4}$, $k_1 = k_2^* = \frac{3}{2}$, $\xi_{01} = \xi_{02} = 0$, $\gamma_1 = -1$, $\gamma_2 = -1$, $\gamma_3 = 1$, $\gamma_4 = 1$, $\gamma_5 = 1$. (a) 3D structure of u; (b) 3D structure of v; (c) 2D density plot of u; (d) 2D density plot of v

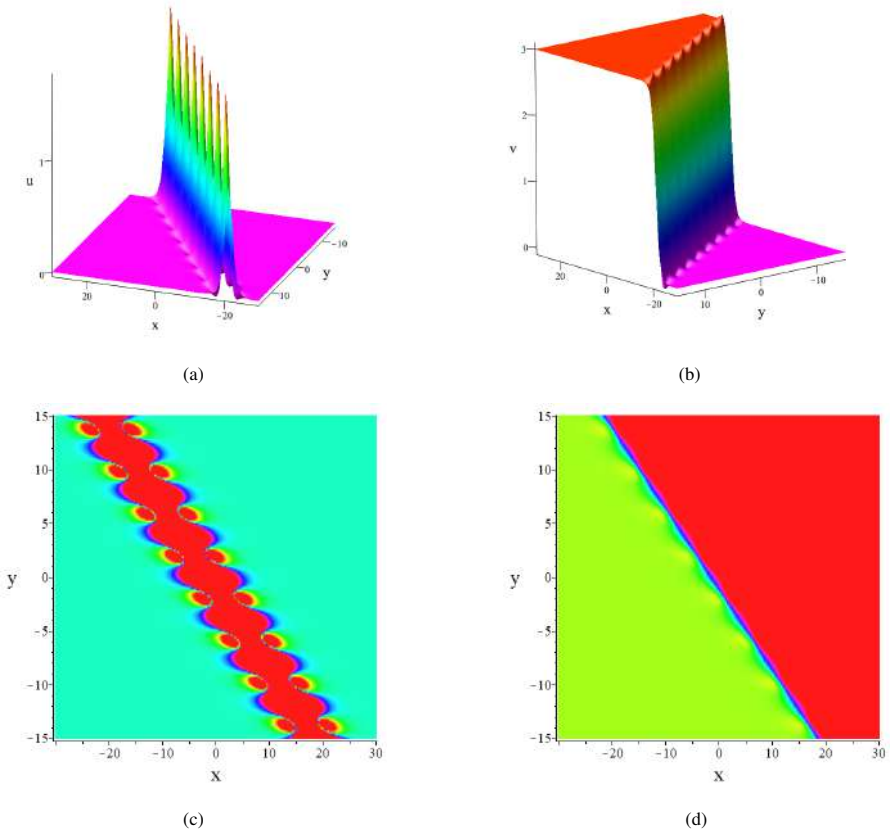

Fig. 4 The (x, y)-periodic and kink breather solition solutions at $t = 0$ when the parameters are chosen as follows: $k_1 = k_2 = \frac{3}{4}$, $s_1 = s_2^* = 1 + \frac{8}{5}i$, $\xi_{01} = \xi_{02} = 0$, $\gamma_1 = -1$, $\gamma_2 = -1$, $\gamma_3 = 1$, $\gamma_4 = 1$, $\gamma_5 = 1$. (a) 3D structure of u; (b) 3D structure of v; (c) 2D density plot of u; (d) 2D density plot of v

solutions u and v at $t = 0$, which are displayed in Figs. 5a and 5c respectively. It can be clearly observed from Fig. 5a that this soliton has two minima and one maximum while 5c shows that it is symmetrical about the central point $(0, 0)$. Correspondingly, Figs. 5b and 5d present the three-dimensional plot and density plot of the soliton v. Unlike soliton u, v presents a maximum and a minimum in the three-dimensional plot 5b, but its density plot 5d is also symmetrical about the center $(0, 0)$.

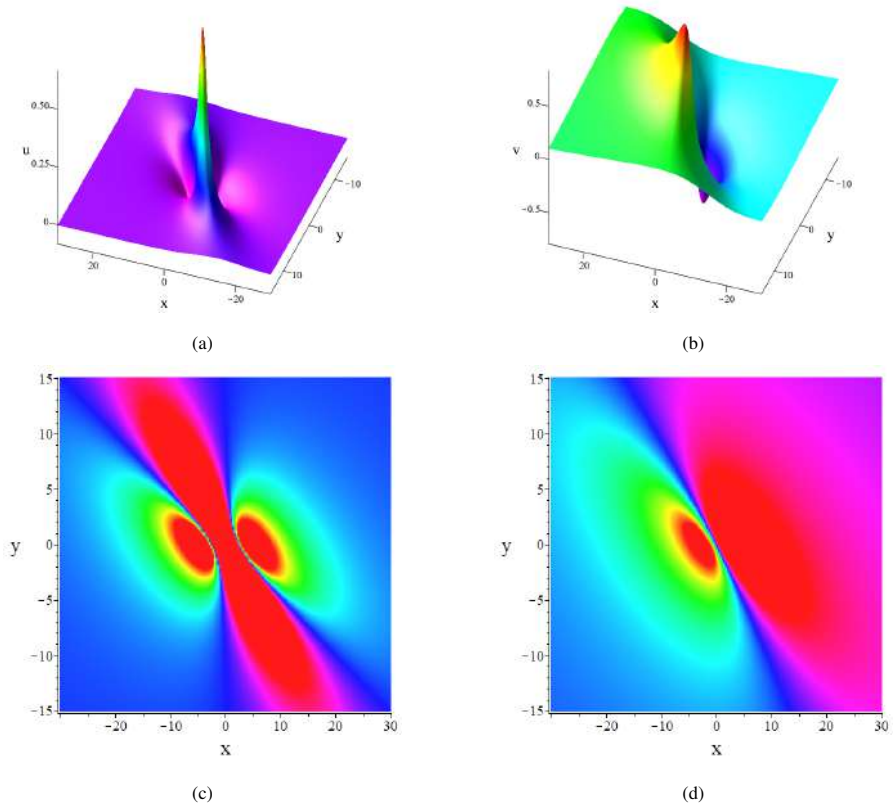

Fig. 5 The lump soliton at $t = 0$ when the parameters are chosen as follows: $k_1 = k_2 = 0.01$, $s_1 = s_2^* = 0.01 + 0.01i$, $\xi_{01} = \xi_{02} = i\pi$, $\gamma_1 = -1$, $\gamma_2 = -1$, $\gamma_3 = 1$, $\gamma_4 = 1$, $\gamma_5 = 1$. (a) 3D structure of u; (b) 3D structure of v; (c) 2D density plot of u; (d) 2D density plot of v

The aforementioned results are summarized in Table 1. It is evident from the table that the two-soliton solutions degenerates into various localized wave solutions for different parameter values. This table describes how the local wave structure (second column) of the N-soliton solution (first column) varies with different parameters (third column).

Table 1 The localized wave patterns for two soliton solutions.

N-soliton	**Localized waves patterns**	**Variable values**
N = 2	The bell-shaped and kink solitons	$k_1 = 4,\ k_2 = 1,\ s_1 = 2, s_2 = 3, \xi_{01} = \xi_{02} = 0,$ $\gamma_1 = \gamma_2 = \gamma_3 = \gamma_4 = \gamma_5 = 2$
	The y-period and kink period solitons	$k_1 = k_2 = \frac{3}{4},\ s_1 = \frac{3}{2}i, s_1 = -\frac{3}{2}i, \xi_{01} = \xi_{02} = 0,$ $\gamma_1 = \gamma_2 = -1,\ \gamma_3 = \gamma_4 = \gamma_5 = 1$
	The (x, y)-period and kink-breather solitons	$k_1 = k_2 = \frac{3}{4},\ s_1 = s_2^* = 1 + \frac{8}{5}i, \xi_{01} = \xi_{02} = 0,$ $\gamma_1 = \gamma_2 = -1,\ \gamma_3 = \gamma_4 = \gamma_5 = 1$
	The lump soltion	$k_1 = k_2 = 0.01,\ s_1 = 0.01 + 0.01i,\ s_2 = 0.01 - 0.01i,\ \xi_{01} = \xi_{02} = i\pi,$ $\gamma_1 = \gamma_2 = -1,\ \gamma_3 = \gamma_4 = \gamma_5 = 1$

2.3 The three-soliton solutions

We set $N = 3$, and the expression of the function f can be obtained by virtue of Eq. (7), written as

$$\begin{aligned} f =& 1 + \exp(\xi_1) + \exp(\xi_2) + \exp(\xi_3) + A_{12}\exp(\xi_1 + \xi_2) \\ &+ A_{13}\exp(\xi_1 + \xi_3) + A_{23}\exp(\xi_2 + \xi_3) + A_{123}\exp(\xi_1 + \xi_2 + \xi_3), \end{aligned} \tag{16}$$

where $A_{123} = A_{12}A_{13}A_{23}$.

By virtue of Eq. (3) and Eq. (16), we can obtain the three-soliton solutions of Eq. (1), given as

$$u = 2 \cdot \left[\frac{f_{xx}}{f} - \left(\frac{f_x}{f} \right)^2 \right], \; v = 2 \cdot \frac{f_x}{f}, \tag{17}$$

where

$$\begin{aligned} f_{xx} =& k_1^2 e^{\xi_1} + k_2^2 e^{\xi_2} + k_3^2 e^{\xi_3} + A_{12}(k_1 + k_2)^2 e^{\xi_1+\xi_2} \\ &+ A_{13}(k_1 + k_3)^2 e^{\xi_1+\xi_3} + A_{23}(k_2 + k_3)^2 e^{\xi_2+\xi_3} + A_{123}(k_1 + k_2 + k_3)^2 e^{\xi_1+\xi_2+\xi_3}, \end{aligned}$$

$$\begin{aligned} f_x =& k_1 e^{\xi_1} + k_2 e^{\xi_2} + k_3 e^{\xi_3} + A_{12}(k_1 + k_2) e^{\xi_1+\xi_2} + A_{13}(k_1 + k_3) e^{\xi_1+\xi_3} \\ &+ A_{23}(k_2 + k_3) e^{\xi_2+\xi_3} + A_{123}(k_1 + k_2 + k_3)^2 e^{\xi_1+\xi_2+\xi_3}, \end{aligned}$$

2.3.1 The bell-shaped and kink solitons

Firstly, we consider that all parameters take real number in Eq. (17), such as $k_1 = 3,\ s_1 = 2,\ k_2 = 1,\ s_2 = 3,\ k_3 = 2,\ s_3 = 3,\ \xi_{01} = \xi_{02} = \xi_{03} = 0,\ \gamma_1 = -1,\ \gamma_2 = -1,\ \gamma_3 = 1,\ \gamma_4 = 1,\ \gamma_5 = 1$. By using Maple software, the three soliton solution plots are presented in Fig. 6. It is clearly seen that the solution u exhibits a structure of three interaction bell-shaped solitons, whereas the solution v is characterized by a three-kink soliton.

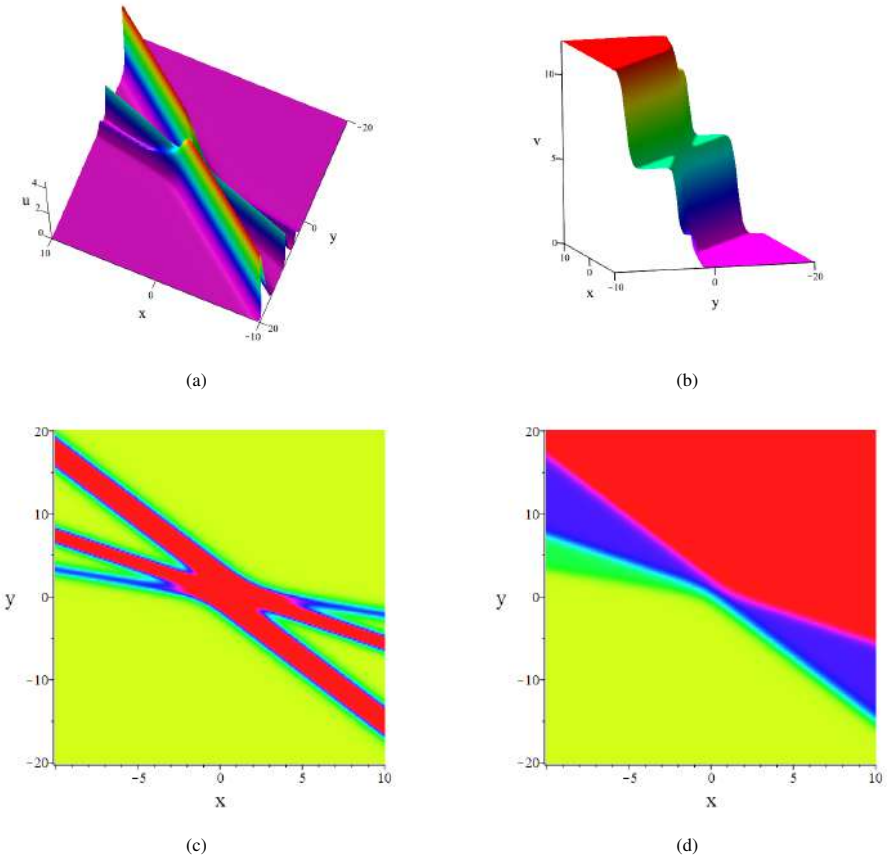

(a) (b)

(c) (d)

Fig. 6 Three-soliton solutions of Eq. (1) at $t = 0$ when the parameters are chosen as follows: $k_1 = 3,\ s_1 = 2,\ k_2 = 1,\ s_2 = 3,\ k_3 = 2,\ s_3 = 3,\ \xi_{01} = \xi_{02} = \xi_{03} = 0,\ \gamma_1 = -1,\ \gamma_2 = -1,\ \gamma_3 = 1,\ \gamma_4 = 1,\ \gamma_5 = 1$. (a) 3D structure of u; (b) 3D structure of v; (c) 2D density plot of u; (d) 2D density plot of v

2.3.2 The line, period and kink solitons (I)

For the three soliton solution in Eq. (17), we set the parameters as $k_1 = k_2 = \frac{7}{8}$, $k_3 = \frac{4}{3}$, $s_1 = \frac{3}{2}i$, $s_2 = -\frac{3}{2}i$, $s_3 = 0$, $\xi_{01} = \xi_{02} = \xi_{03} = 0$, $\gamma_1 = -1$, $\gamma_2 = -1$, $\gamma_3 = 1$, $\gamma_4 = 1$, $\gamma_5 = 1$. We find that the three-soliton can degenerate into other solitons and be expressed as interactions between these solitons. Fig. 7 shows the three-dimensional diagrams and the corresponding density plots of the degenerate three-soliton u moving over time. It can be observed that the three-soliton u degenerates into a bell-shaped line soliton and a periodic soliton which parallel to the y-axis, they all propagate in the negative x-direction. The y-periodic soliton moves at a higher speed. At $t = 0$, they collided. After the collision, neither their shapes nor their velocities show significant changes, but their positions are exchanged. Fig. 8 presents those of the degenerate three-soliton v. It can be observed from Fig. 8 that the three-soliton v degenerates into a two-kink periodic soliton and a one-kink soliton, both of which are orthogonal to the x-axis. Looking at Figs. 7 and 8 as a whole, we find that the other solitons formed by the degeneration of the three-soliton do not change their shapes after colliding with each other. We refer to this type of collision as an elastic mutual collision.

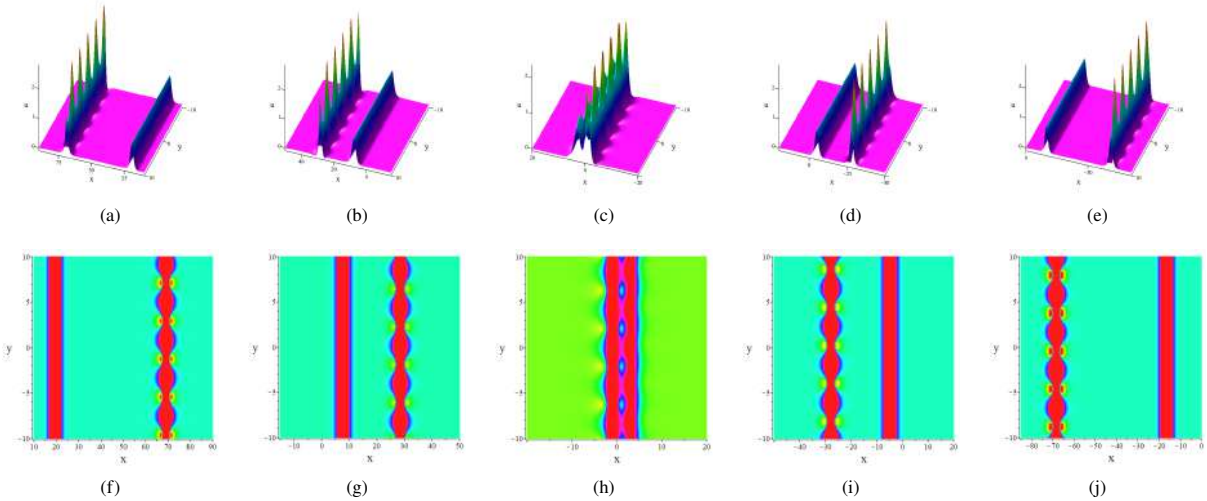

Fig. 7 One line soliton and periodic soliton which parallel to the y-axis of Eq. (1) at different time when the parameters are chosen as follows: $k_1 = k_2 = \frac{7}{8}$, $k_3 = \frac{4}{3}$, $s_1 = \frac{3}{2}i$, $s_2 = -\frac{3}{2}i$, $s_3 = 0$, $\xi_{01} = \xi_{02} = \xi_{03} = 0$, $\gamma_1 = -1$, $\gamma_2 = -1$, $\gamma_3 = 1$, $\gamma_4 = 1$, $\gamma_5 = 1$. (a)-(e) 3D structure of u; (f)-(j) 2D structure of u; (a)(f)$t = -25$; (b)(g)$t = -10$; (c)(h)$t = 0$; (d)(i)$t = 10$; (e)(j)$t = 25$

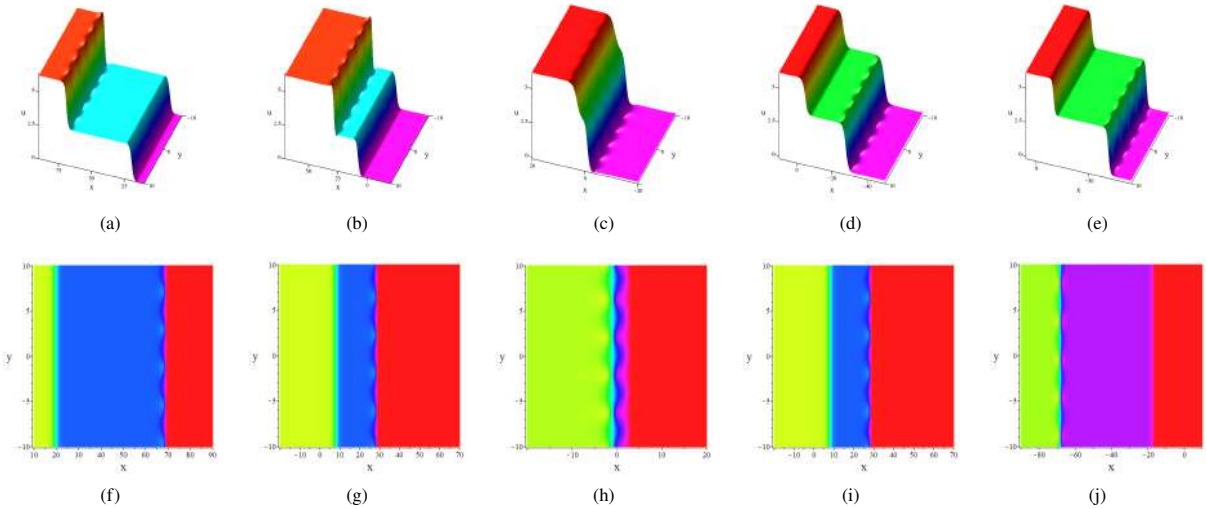

Fig. 8 One kink periodic soliton and one-kink soliton of Eq. (1) at different time when the parameters are chosen as follows: $k_1 = \frac{7}{8}$, $k_2 = \frac{7}{8}$, $k_3 = \frac{4}{3}$, $s_1 = \frac{3}{2}i$, $s_2 = -\frac{3}{2}i$, $s_3 = 0$, $\xi_{01} = \xi_{02} = \xi_{03} = 0$, $\gamma_1 = -1$, $\gamma_2 = -1$, $\gamma_3 = 1$, $\gamma_4 = 1$, $\gamma_5 = 1$. (a)-(e) 3D structure of v; (f)-(j) 2D structure of v; (a)(f)$t = -25$; (b)(g)$t = -10$; (c)(h)$t = 0$; (d)(i)$t = 10$; (e)(j)$t = 25$

2.3.3 The line, period and kink solitons (II)

In this subsection, the parameters are set to $k_1 = k_2 = \frac{7}{8}$, $k_3 = \frac{4}{3}$, $s_1 = \frac{3}{2}i$, $s_2 = -\frac{3}{2}i$, $s_3 = 1$, $\xi_{01} = \xi_{02} = \xi_{03} = 0$, $\gamma_1 = -1$, $\gamma_2 = -1$, $\gamma_3 = 1$, $\gamma_4 = 1$, $\gamma_5 = 1$. Noted that $s_3 \neq 0$ (different from 2.3.2), it can be observed the three soliton u degenerates into a line soliton and a periodic soliton. On the other hand, the three-soliton v degenerates into a two-kink periodic soliton and a one-kink soliton. The corresponding three-dimensional structures and density distributions are shown in Fig. 9 and Fig. 10, respectively. As observed in Fig. 9, the periodic soliton maintains a perpendicular orientation to the x-axis while propagating in the negative x-direction, while the line soliton moves from the upper right to lower left in the (x, y) plane. The results in Fig. 10 show that the two-kink periodic soliton is also perpendicular to the x-axis, and its waveform propagates in the negative x-direction, whereas the one-kink soliton moves from the lower left to the upper right in the (x, y) plane. Both figures demonstrate that the degenerated soliton solutions u and v maintain their structural integrity throughout the crossing interaction, this observation confirms that the collision is elastic.

2.3.4 The lump, line and kink solitons

For the Eq. (17), the parameters take the following values: $k_1 = 0.01$, $k_2 = 1$, $k_3 = 0.01$, $s_1 = 0.01 + 0.01i$, $s_2 = 1$, $s_3 = 0.01 - 0.01i$, $\xi_{01} = \xi_{02} = \xi_{03} = i\pi$, $\gamma_1 = -1$, $\gamma_2 = -1$, $\gamma_3 = 1$, $\gamma_4 = 1$, $\gamma_5 = 1$. By employing Maple software, the structure pattern of the soliton solution can be exhibited graphically. Specifically, soliton u evolves into a lump soliton and a bell-shaped line soliton, while soliton v transforms into a lump soliton and a one- kink soliton. In this subsection, we focus on presenting their time-evolution density plots, as specifically illustrated in Fig. 11 (for soliton u) and Fig. 12 (for soliton v). To better observe their collision dynamics, five distinct time instants ($t = -30$, $t = -10$, $t = 0$, $t = 10$, $t = 30$) were selected, corresponding to subfigures a - e, respectively. It can be distinctly observed from Fig. 11 that both the bell-shaped line soliton and the lump soliton propagate from the lower right to the upper left in the (x, y) plane, and the bell-shaped line soliton moves significantly faster than the lump soliton. Over time, the line soliton catches up with the lump soliton. At time $t = 0$, the two solitons spatially coincide and undergo a mutual collision. After the collision, neither exhibits morphological distortion or velocity change. Instead, they continue propagating along their original trajectories. The dynamical behavior of soliton v shown in Fig. 12 is similar to that of u, and thus a detailed description is omitted here for brevity. It is noted that the collision between these two different types of solitons are also confirmed to be elastic.

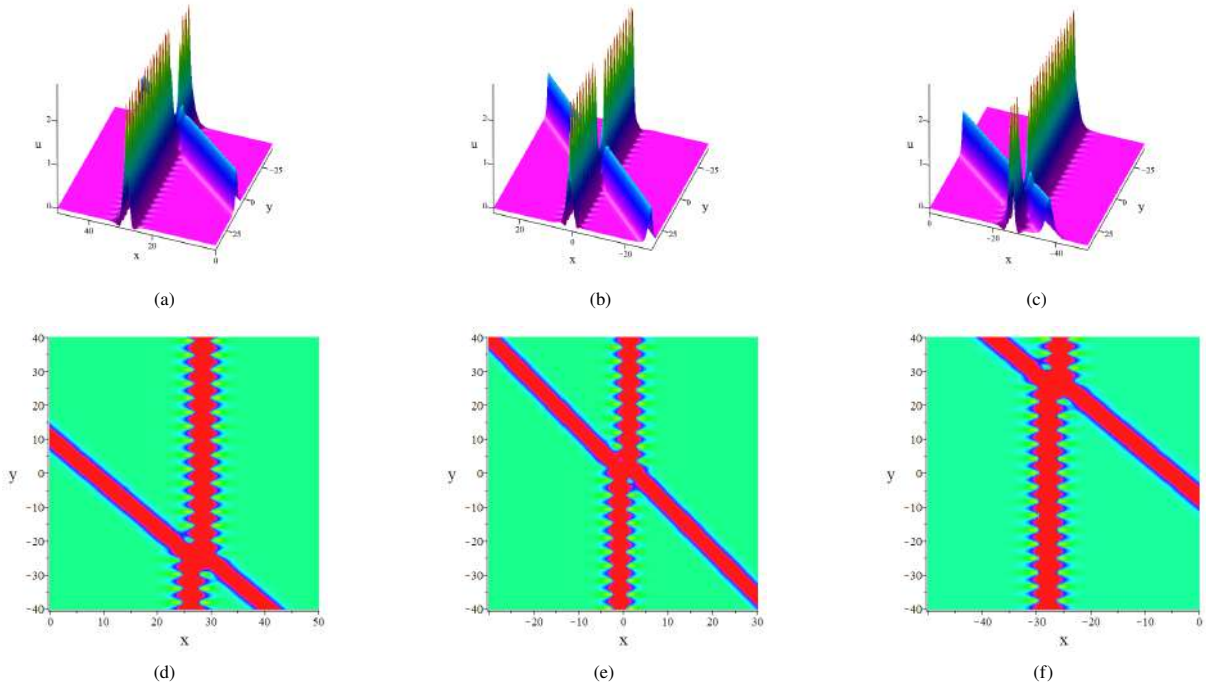

Fig. 9 One line soliton and one periodic soliton of Eq. (1) at different time when the parameters are chosen as follows: $k_1 = k_2 = \frac{7}{8}$, $k_3 = \frac{4}{3}$, $s_1 = \frac{3}{2}i$, $s_2 = -\frac{3}{2}i$, $s_3 = 1$, $\xi_{01} = \xi_{02} = \xi_{03} = 0$, $\gamma_1 = -1$, $\gamma_2 = -1$, $\gamma_3 = 1$, $\gamma_4 = 1$, $\gamma_5 = 1$; (a)-(c) 3D structure of u; (d)-(f) 2D structure of u; (a)(d)$t = -10$; (b)(e)$t = 0$; (c)(f)$t = 10$

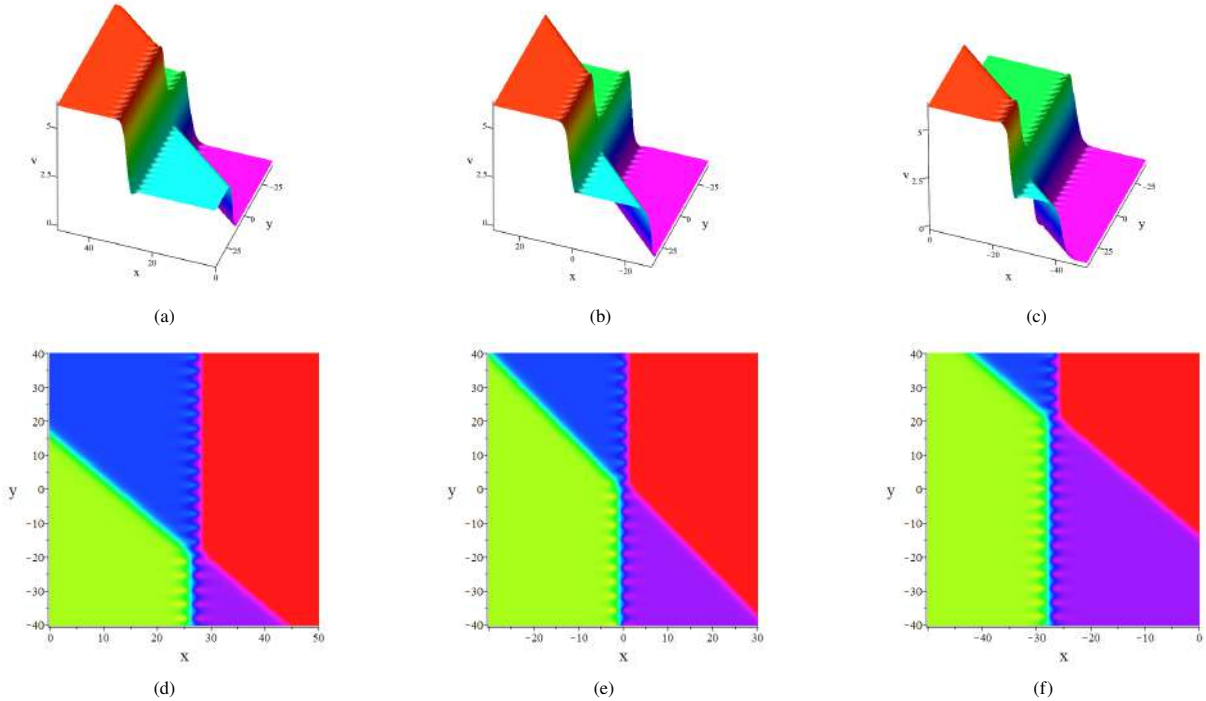

Fig. 10 One kink soliton and two-kink periodic soliton of Eq. (1) at different time when the parameters are chosen as follows: $k_1 = k_2 = \frac{7}{8}$, $k_3 = \frac{4}{3}$, $s_1 = \frac{3}{2}i$, $s_2 = -\frac{3}{2}i$, $s_3 = 1$, $\xi_{01} = \xi_{02} = \xi_{03} = 0$, $\gamma_1 = -1$, $\gamma_2 = -1$, $\gamma_3 = 1$, $\gamma_4 = 1$, $\gamma_5 = 1$; (a)-(c) 3D structure of v; (d)-(f) 2D structure of v; (a)(d)$t = -10$; (b)(e)$t = 0$; (c)(f)$t = 10$

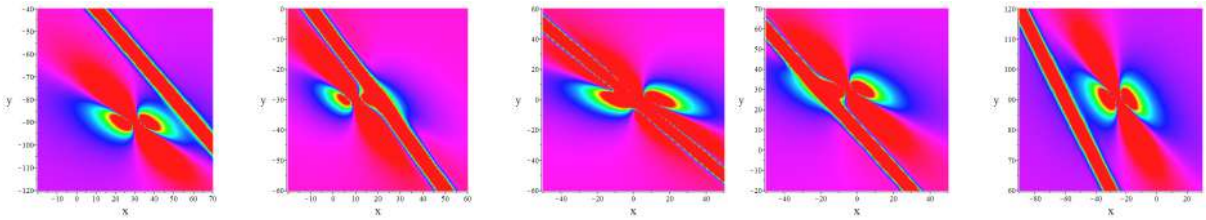

Fig. 11 One line soliton and one lump soliton of Eq. (1) at different time for the following parameter values: $k_1 = 0.01$, $k_2 = 1$, $k_3 = 0.01$, $s_1 = 0.01+0.01i$, $s_2 = 1$, $s_3 = 0.01 - 0.01i$, $\xi_{01} = \xi_{02} = \xi_{03} = i\pi$, $\gamma_1 = -1$, $\gamma_2 = -1$, $\gamma_3 = 1$, $\gamma_4 = 1$, $\gamma_5 = 1$. (a)-(e) 2D structure of u; (a)$t = -30$; (b)$t = -10$; (c)$t = 0$; (d)$t = 10$; (e)$t = 30$

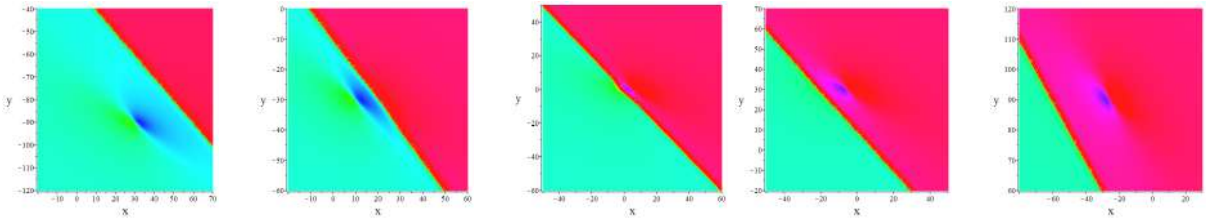

Fig. 12 One lump soliton and one kink soliton of Eq. (1) at different time, for the following parameter values: $k_1 = 0.01$, $k_2 = 1$, $k_3 = 0.01$, $s_1 = 0.01 + 0.01i$, $s_2 = 1$, $s_3 = 0.01 - 0.01i$, $\xi_{01} = \xi_{02} = \xi_{03} = i\pi$, $\gamma_1 = -1$, $\gamma_2 = -1$, $\gamma_3 = 1$, $\gamma_4 = 1$, $\gamma_5 = 1$. (a)-(e) 2D structure of v; (a)$t = -30$; (b)$t = -10$; (c)$t = 0$; (d)$t = 10$; (e)$t = 30$

Table 2 summarizes localized waves and the interaction relationships for the three-soliton solutions, presenting four types of interactions discussed in this paper. This table describes how the local wave structure (second column) of the N-soliton solution (first column) varies with different parameters (third column).

Table 2 The localized wave patterns for three soliton solutions

N-soliton	Localized waves patterns	Variable values
N = 3	The bell-shaped and kink solitons	$k_1 = 3,\ k_2 = 1,\ s_1 = 2,\ s_2 = 3,\ k_3 = 2,\ s_3 = 3, \xi_{01} = \xi_{02} = \xi_{03} = 0,$ $\gamma_1 = \gamma_2 = -1,\ \gamma_3 = \gamma_4 = \gamma_5 = 1$
	The line, period and kink solitons (I)	$k_1 = k_2 = \frac{7}{8},\ s_1 = s_2^* = \frac{3}{2}i,\ k_3 = \frac{4}{3},\ s_3 = 0,$ $\xi_{01} = \xi_{02} = \xi_{03} = 0,$ $\gamma_1 = \gamma_2 = -1,\ \gamma_3 = \gamma_4 = \gamma_5 = 1$
	The line, period and kink solitons (II)	$k_1 = k_2 = \frac{7}{8},\ s_1 = s_2^* = \frac{3}{2}i,\ k_3 = \frac{4}{3},\ s_3 = 1,$ $\xi_{01} = \xi_{02} = \xi_{03} = 0,$ $\gamma_1 = \gamma_2 = -1,\ \gamma_3 = \gamma_4 = \gamma_5 = 1$
	The lump, line and kink solitons	$k_1 = k_3 = 0.01,\ k_2 = 1,\ s_1 = 0.01 + 0.01i,\ s_2 = 1,\ s_3 = 0.01 - 0.01i,\ \xi_{01} = \xi_{02} = \xi_{03} = i\pi,$ $\gamma_1 = \gamma_2 = -1,\ \gamma_3 = \gamma_4 = \gamma_5 = 1$

2.4 Four soliton solutions

We set $N = 4$, and the following formula can be obtained from Eq. (7)

$$\begin{aligned} f =& 1 + \exp(\xi_1) + \exp(\xi_2) + \exp(\xi_3) + \exp(\xi_4) + A_{12}\exp(\xi_1 + \xi_2) + A_{13}\exp(\xi_1 + \xi_3) \\ &+ A_{14}\exp(\xi_1 + \xi_4) + A_{23}\exp(\xi_2 + \xi_3) + A_{24}\exp(\xi_2 + \xi_4) + A_{34}\exp(\xi_3 + \xi_4) \\ &+ A_{123}\exp(\xi_1 + \xi_2 + \xi_3) + A_{124}\exp(\xi_1 + \xi_2 + \xi_4) + A_{134}\exp(\xi_1 + \xi_3 + \xi_4) \\ &+ A_{234}\exp(\xi_2 + \xi_3 + \xi_4) + A_{1234}\exp(\xi_1 + \xi_2 + \xi_3 + \xi_4), \end{aligned} \tag{18}$$

where $A_{1234} = A_{12}A_{13}A_{14}A_{23}A_{24}A_{34}$. By virtue of Eq. (3) and Eq. (18), we can obtain the four-soliton solutions of Eq. (1). Since the expressions of soliton solutions are too complicated, they are omitted here.

2.4.1 The bell and kink solitons

In this subsection, we consider that the parameter values $k_1 = 3,\ s_1 = 1,\ k_2 = 1,\ s_2 = 3,\ k_3 = 1,\ s_3 = 1,\ k_4 = 2,\ s_4 = 3,\ \eta_{01} = \eta_{02} = \eta_{03} = \eta_{04} = 0, \gamma_1 = -1,\ \gamma_2 = -1,\ \gamma_3 = 1,\ \gamma_4 = 1,\ \gamma_5 = 1$. The four-soliton solutions for component u manifests as four bell-shaped line solitons, with its three-dimensional and density plots displayed in Fig. 13. Panel Figs. 13a–e represent the three-dimensional plots, while Figs. 13f-j depict the corresponding density plots. To observe their temporal evolution, five distinct time instants ($t = -10,\ t = -5, t = 0, t = 5,\ t = 10$) are selected from left to right. In contrast, component v evolves into a four-kink soliton, illustrated in Fig. 14 under the same conditions as component u. From Fig. 14, it can be clearly observed that the kink positions of the soliton v vary over time.

2.4.2 The line, period and kink solitons

When the parameter values are set as: $k_1 = \frac{3}{4},\ k_2 = \frac{3}{4},\ k_3 = \frac{4}{3},\ k_4 = \frac{4}{3},\ s_1 = \frac{3}{2}i,\ s_2 = -\frac{3}{2}i,\ s_3 = 2,\ s_4 = -2,\ \xi_{01} = \xi_{02} = \xi_{03} = \xi_{04} = 0,\ \gamma_1 = -1,\ \gamma_2 = -1,\ \gamma_3 = 1,\ \gamma_4 = 1,\ \gamma_5 = 1$, the four-soliton solution u displays a structure comprising a periodic soliton along the y-direction and two bell-shaped line solitons while v exhibits a periodic kink soliton along the y-direction and a three-kink soliton. Numerical simulations yield three-dimensional structural plots and density profiles, illustrating the temporal evolution of the degenerate solitons u and v, clearly demonstrating their dynamic interaction process. Fig. 15 shows the interaction of u over time, while Fig. 16 corresponds to that of v. From these figures, it can be clearly observed that despite variations in time t, the solitons maintain their original morphology and dynamic characteristics after collision. This phenomenon confirms that the interaction between such solitons is a typical elastic interaction, adhering to momentum and energy conservation during the collision process and exhibiting strong stability.

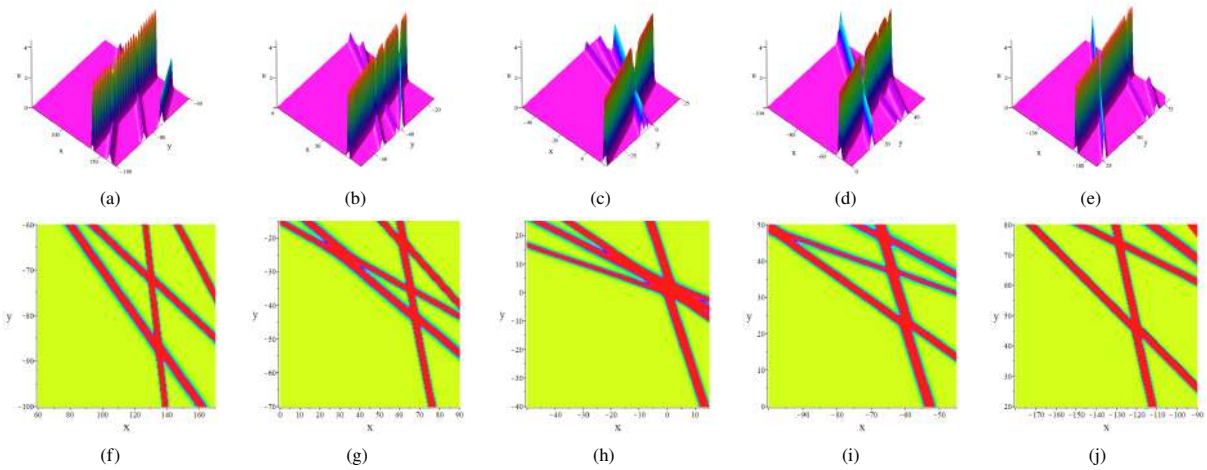

Fig. 13 Four soliton solutions of Eq. (1) at different time when the parameters are chosen as follows: $k_1 = 3,\ s_1 = 1,\ k_2 = 1,\ s_2 = 3,\ k_3 = 1,\ s_3 = 1,\ k_4 = 2,\ s_4 = 3,\ \xi_{01} = \xi_{02} = \xi_{03} = \xi_{04} = 0,\ \gamma_1 = -1,\ \gamma_2 = -1,\ \gamma_3 = 1,\ \gamma_4 = 1,\ \gamma_5 = 1$. (a)-(e) 3D structure of u; (f)-(j) 2D structure of u; (a)(f)$t = -10$; (b)(g)$t = -5$; (c)(h)$t = 0$; (d)(i)$t = 5$; (e)(j)$t = 10$

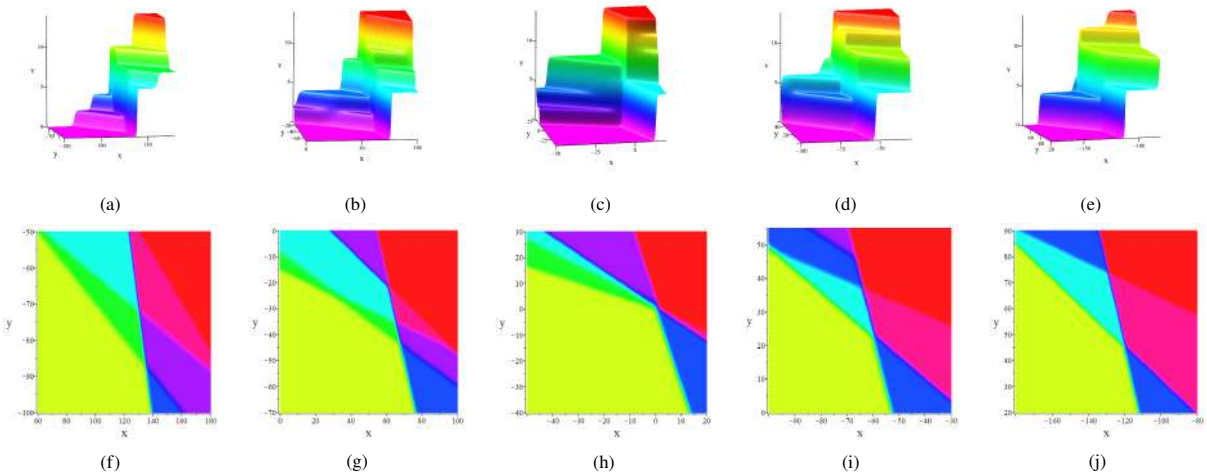

Fig. 14 Four soliton solutions of Eq. (1) at different time when the parameters are chosen as follows: $k_1 = 3,\ s_1 = 1,\ k_2 = 1,\ s_2 = 3,\ k_3 = 1,\ s_3 = 1,\ k_4 = 2,\ s_4 = 3,\ \xi_{01} = \xi_{02} = \xi_{03} = \xi_{04} = 0,\ \gamma_1 = -1,\ \gamma_2 = -1,\ \gamma_3 = 1,\ \gamma_4 = 1,\ \gamma_5 = 1$. (a)-(e) 3D structure of v; (f)-(j) 2D structure of v; (a)(f)$t = -10$; (b)(g)$t = -5$; (c)(h)$t = 0$; (d)(i)$t = 5$; (e)(j)$t = 10$

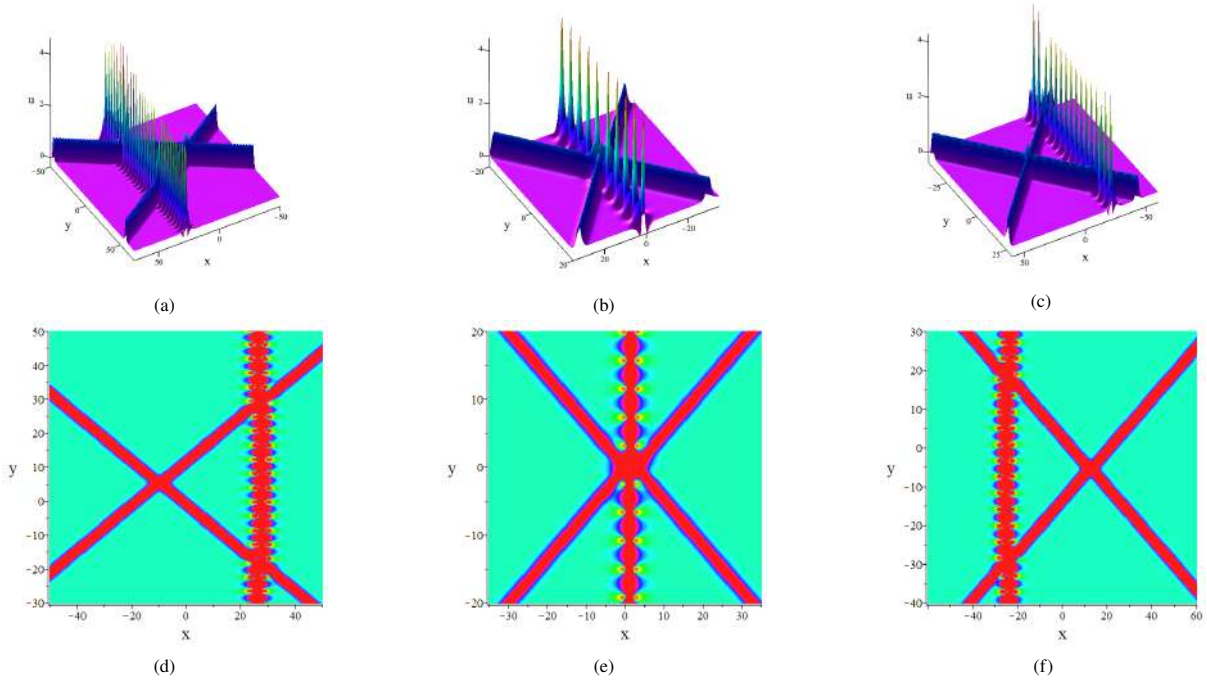

Fig. 15 Two line solitons and one y-periodic soliton at different time when the parameters are chosen as follows: $k_1 = k_2 = \frac{3}{4},\ k_3 = k_4 = \frac{4}{3},\ s_1 = \frac{3}{2}i,\ s_2 = -\frac{3}{2}i,\ s_3 = 2,\ s_4 = -2,\ \xi_{01} = \xi_{02} = \xi_{03} = \xi_{04} = 0,\ \gamma_1 = -1,\ \gamma_2 = -1,\ \gamma_3 = 1,\ \gamma_4 = 1,\ \gamma_5 = 1$. (a)-(c) 3D structure of u; (d)-(f) 2D structure of u; (a)(d)$t = -7$; (b)(e)$t = 0$; (c)(f)$t = 7$

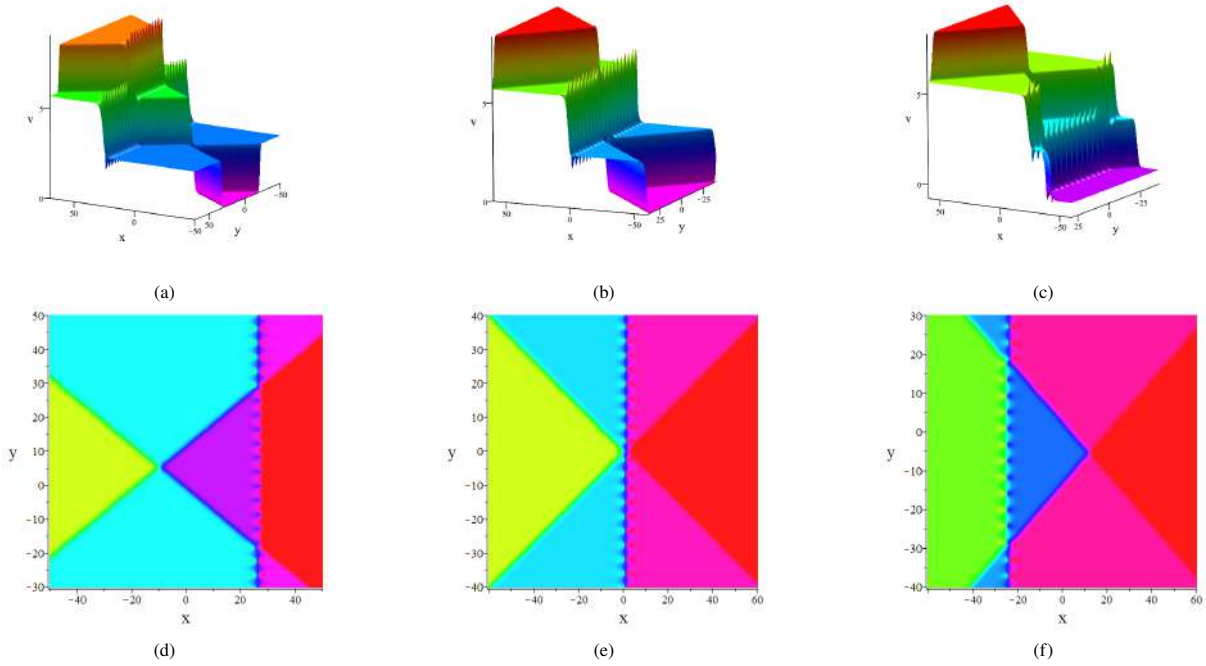

Fig. 16 Two-kink-soliton and one periodic kink soliton at different time when the parameters are chosen as follows: $k_1 = \frac{3}{4}$, $k_2 = \frac{3}{4}$, $k_3 = \frac{4}{3}$, $k_4 = \frac{4}{3}$, $s_1 = \frac{3}{2}i$, $s_2 = -\frac{3}{2}i$, $s_3 = 2, s_4 = -2$, $\xi_{01} = \xi_{02} = \xi_{03} = \xi_{04} = 0$, $\gamma_1 = -1$, $\gamma_2 = -1$, $\gamma_3 = 1$, $\gamma_4 = 1$, $\gamma_5 = 1$. (a)-(c) 3D structure of v; (d)-(f) 2D structure of v; (a)(d)$t = -7$; (b)(e)$t = 0$; (c)(f)$t = 7$

2.4.3 The period and kink period solitons (I)

When the parameters take the values of $k_1 = \frac{3}{4}$, $k_2 = \frac{3}{4}$, $k_3 = \frac{2}{3}$, $k_4 = \frac{2}{3}$, $s_1 = \frac{6}{5}i$, $s_2 = -\frac{6}{5}i$, $s_3 = -\frac{4}{3}i$, $s_4 = \frac{4}{3}i$, $\xi_{01} = \xi_{02} = \xi_{03} = \xi_{04} = 0$, $\gamma_1 = 1$, $\gamma_2 = 1$, $\gamma_3 = -1$, $\gamma_4 = -1$, $\gamma_5 = -1$, a clear degeneration behavior can be observed for the four soliton solution u, which transform into two periodic solitons along the y-direction. The three-dimensional and density plots of these two y-periodic solitons are displayed in Fig. 17. It can be seen that both solitons are observed to propagate along the positive x-axis, with one moving at a relatively higher speed. At $t = 0$, the two solitons undergo a collision. After the collision, they retain their original wave profiles and propagation speeds, continuing to move in the positive x-direction. Simultaneously, the four-soliton v also degenerates into two kink periodic solitons, whose three-dimensional and density plots are depicted in Fig. 18. The motion trajectories of these two kink periodic solitons are highly analogous to those of the soliton u and both exhibit counter propagation, collision, and subsequent separation and thus will not be reiterated here. It is particularly noteworthy that the collision is elastic, which further confirms the reversible and stable nature of such soliton interactions.

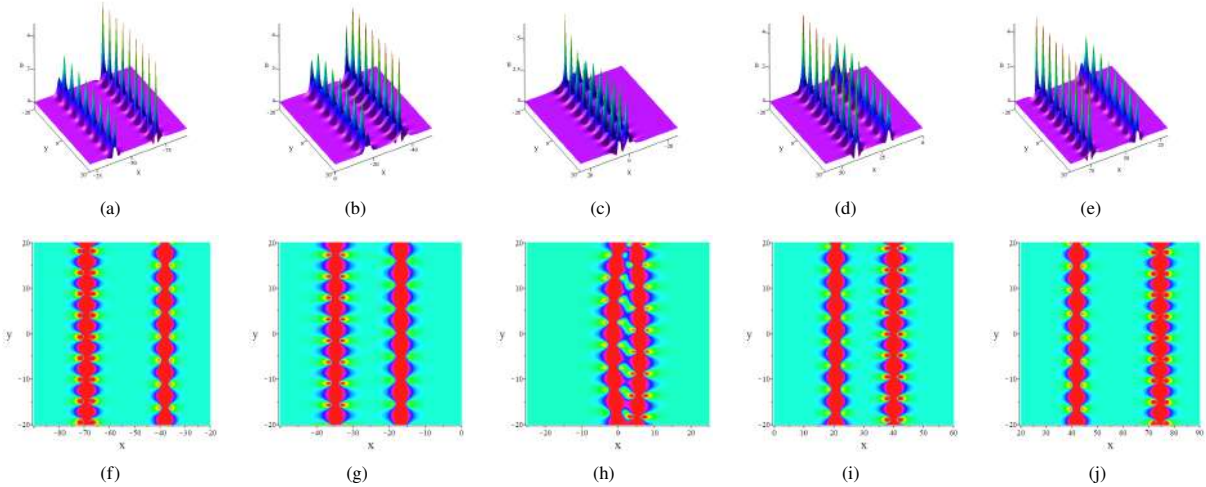

Fig. 17 Two periodic soliton solutions of Eq. (1) at different time when the parameters are chosen as follows: $k_1 = \frac{3}{4}$, $k_2 = \frac{3}{4}$, $k_3 = \frac{2}{3}$, $k_4 = \frac{2}{3}$, $s_1 = \frac{6}{5}i$, $s_2 = -\frac{6}{5}i$, $s_3 = -\frac{4}{3}i$, $s_4 = \frac{4}{3}i$, $\xi_{01} = \xi_{02} = \xi_{03} = \xi_{04} = 0$, $\gamma_1 = 1$, $\gamma_2 = 1$, $\gamma_3 = -1$, $\gamma_4 = -1$, $\gamma_5 = -1$. (a)-(e) 3D structure of u; (f)-(j) 2D structure of u, (a)(f)$t = -20$; (b)(g)$t = -10$; (c)(h)$t = 0$; (d)(i)$t = 10$; (e)(j)$t = 20$

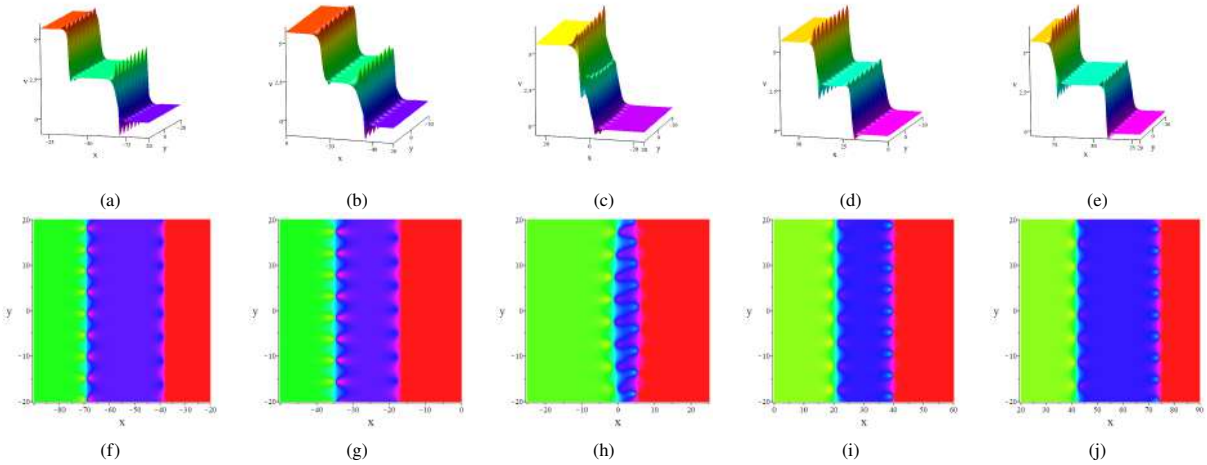

Fig. 18 Two kink periodic soliton solutions of Eq. (1) at different time when the parameters are chosen as follows: $k_1 = \frac{3}{4},\ k_2 = \frac{3}{4},\ k_3 = \frac{2}{3},\ k_4 = \frac{2}{3},\ s_1 = \frac{6}{5}i,\ s_2 = -\frac{6}{5}i,\ s_3 = -\frac{4}{3}i,\ s_4 = \frac{4}{3}i,\ \xi_{01} = \xi_{02} = \xi_{03} = \xi_{04} = 0,\ \gamma_1 = 1,\ \gamma_2 = 1,\ \gamma_3 = -1,\ \gamma_4 = -1,\ \gamma_5 = -1$. (a)-(e) 3D structure of v; (f)-(j) 2D structure of v, (a)(f)$t = -20$; (b)(g)$t = -10$; (c)(h)$t = 0$; (d)(i)$t = 10$; (e)(j)$t = 20$

2.4.4 The period and kink period solitons (II)

When the parameters values are taken as $k_1 = \frac{3}{4},\ k_2 = \frac{3}{4},\ k_3 = \frac{2}{3},\ k_4 = \frac{2}{3},\ s_1 = \frac{6}{5}i,\ s_2 = -\frac{6}{5}i,\ s_3 = 1 - \frac{4}{3}i,\ s_4 = 1 + \frac{4}{3}i,\ \xi_{01} = \xi_{02} = \xi_{03} = \xi_{04} = 0,\ \gamma_1 = 1,\ \gamma_2 = 1,\ \gamma_3 = -1,\ \gamma_4 = -1,\ \gamma_5 = -1$, a new kind of four soliton solutions u and v can be obtained, as shown in Fig. 19 and Fig. 20, respectively. From Fig. 19, it can be observed that the four-soliton u decomposes into two periodic solitons: one parallel to the y-axis and the other intersecting the y-axis. Furthermore the interaction between them is also demonstrated. We find that the (x, y)-periodic soliton in this case propagates diagonally from the lower left to the upper right within the (x, y) plane, while the y-periodic soliton continues to travel along the positive x-axis direction. Fig. 20 shows the interaction between one y-periodic kink soliton and one (x, y)-periodic kink soliton for the solution v, this interaction is very similar to those of solution u and the corresponding description is omitted. For both figures, panels a-e and f-j display the three-dimensional structures and their corresponding density plots, respectively. The selected time points are set to $t = -10$, $t = -5$, $t = 0$, $t = 5$, $t = 10$ in increasing order from left to right.

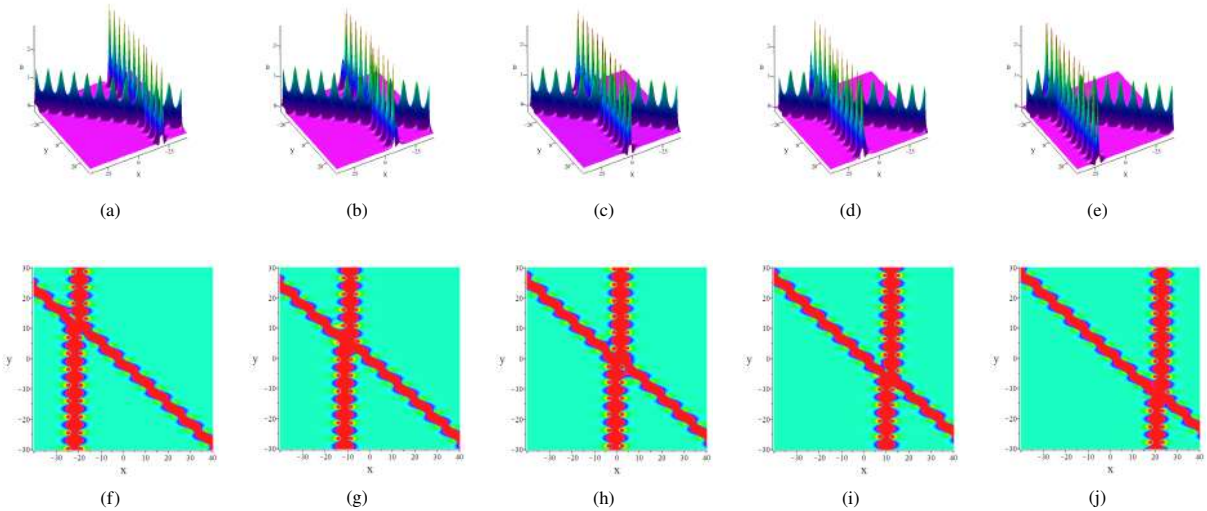

Fig. 19 One y-periodic soliton and one (x, y)-periodic soliton of Eq. (1) at different time when the parameters are chosen as follows: $k_1 = \frac{3}{4},\ k_2 = \frac{3}{4},\ k_3 = \frac{2}{3},\ k_4 = \frac{2}{3},\ s_1 = \frac{6}{5}i,\ s_2 = -\frac{6}{5}i,\ s_3 = 1 - \frac{4}{3}i,\ s_4 = 1 + \frac{4}{3}i,\ \xi_{01} = \xi_{02} = \xi_{03} = \xi_{04} = 0,\ \gamma_1 = 1,\ \gamma_2 = 1,\ \gamma_3 = -1,\ \gamma_4 = -1,\ \gamma_5 = -1$. (a)-(e) 3D structure of u; (f)-(j) 2D structure of u, (a)(f)$t = -10$; (b)(g)$t = -5$; (c)(h)$t = 0$; (d)(i)$t = 5$; (e)(j)$t = 10$

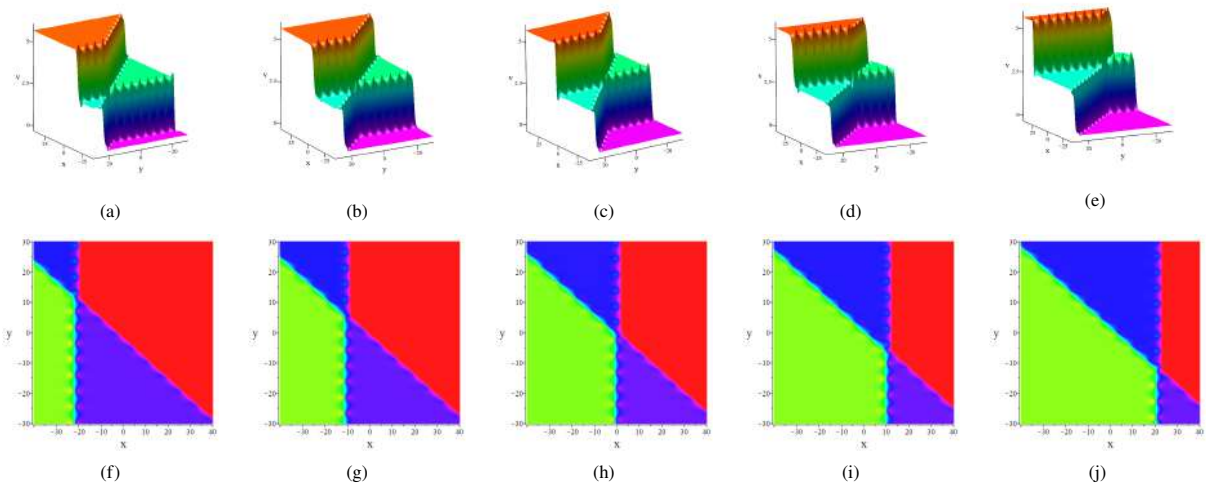

Fig. 20 One y-periodic kink soliton and one (x, y)-periodic kink soliton of Eq. (1) at different time when the parameters are chosen as follows: $k_1 = \frac{3}{4}$, $k_2 = \frac{3}{4}$, $k_3 = \frac{2}{3}$, $k_4 = \frac{2}{3}$, $s_1 = \frac{6}{5}i$, $s_2 = -\frac{6}{5}i$, $s_3 = 1 - \frac{4}{3}i$, $s_4 = 1 + \frac{4}{3}i$, $\xi_{01} = \xi_{02} = \xi_{03} = \xi_{04} = 0$, $\gamma_1 = 1$, $\gamma_2 = 1$, $\gamma_3 = -1$, $\gamma_4 = -1$, $\gamma_5 = -1$. (a)-(e) 3D structure of v; (f)-(j) 2D structure of v, (a)(f)$t = -10$; (b)(g)$t = -5$; (c)(h)$t = 0$; (d)(i)$t = 5$; (e)(j)$t = 10$

2.4.5 Multi-lump solitons

When the parameter values are set as $k_1 = k_2 = 0.01, s_1 = s_2^* = 0.01+0.01i, k_3 = k_4 = 0.02, s_3 = s_4^* = 0.02+0.02i$, $\xi_{01} = \xi_{02} = \xi_{03} = \xi_{04} = i\pi, \gamma_1 = -1, \gamma_2 = -1, \gamma_3 = 1, \gamma_4 = 1, \gamma_5 = 1$, the four-soliton solutions can be observed to degenerate into a series of lump solitons structures. These lump solitons exhibit rich distribution patterns on the (x, y) plane. Figs. 21a and 21c show the three-dimensional morphology and the corresponding density distribution of soliton u, respectively, Figs. 21b and 21d display the three-dimensional structure and density distribution of soliton v, respectively. Among them, these lump solitons are distributed along the diagonal of the (x, y) plane from upper left to lower right.

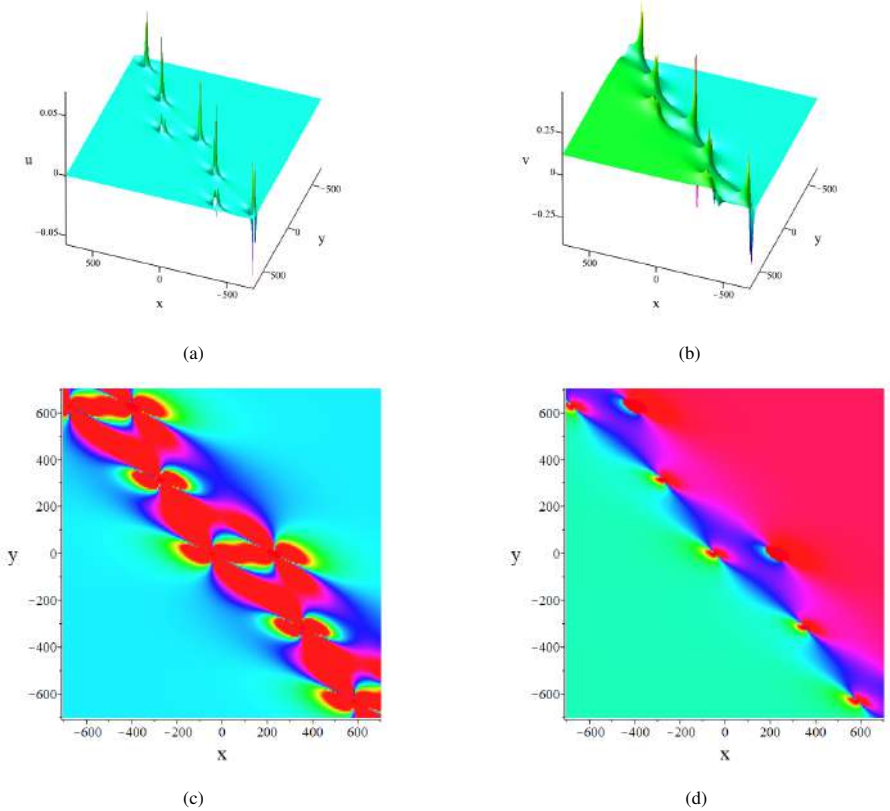

Fig. 21 Multi lump solitons of Eq. (1) at $t = 0$ when the parameters are chosen as follows: $k_1 = k_2 = 0.01$, $s_1 = s_2^* = 0.01 + 0.01i$, $k_3 = k_4 = 0.02$, $s_3 = s_4^* = 0.02 + 0.02i$, $\xi_{01} = \xi_{02} = \xi_{03} = \xi_{04} = i\pi$, $\gamma_1 = -1$, $\gamma_2 = -1$, $\gamma_3 = 1$, $\gamma_4 = 1$, $\gamma_5 = 1$. (a) 3D structure of u; (b) 3D structure of v; (c) 2D density plot of u; (d) 2D density plot of v

Table 3 summarizes the relationship between the local wave patterns and the parameters, which is very meaningful for controlling the wave structures of nonlinear integrable systems.

Table 3 The localized wave patterns for four soliton solutions

N-soliton	**Localized waves patterns**	**Variable values**
N = 4	The bell and kink solitons	$k_1 = 3,\ k_2 = 1,\ s_1 = 1,\ s_2 = 3,\ k_3 = 1,\ k_4 = 3,\ s_3 = 21, s_4 = 3,$ $\xi_{01} = \xi_{02} = \xi_{03} = \xi_{04} = 0,$ $\gamma_1 = \gamma_2 = -1, \gamma_3 = \gamma_4 = \gamma_5 = 1$
	The line, period and kink solitons	$k_1 = k_2 = \frac{3}{4},\ s_1 = -\frac{3}{2}i,\ s_2 = \frac{3}{2}i,\ k_3 = k_4 = \frac{4}{3},\ s_3 = 2, s_4 = -2,$ $\xi_{01} = \xi_{02} = \xi_{03} = \xi_{04} = 0,$ $\gamma_1 = \gamma_2 = -1, \gamma_3 = \gamma_4 = \gamma_5 = 1$
	The period and kink period solitons (I)	$k_1 = k_2 = \frac{3}{4},\ s_1 = \frac{6}{5}i,\ s_2 = -\frac{6}{5}i,\ k_3 = k_4 = \frac{2}{3},\ s_3 = -\frac{4}{3}i,\ s_4 = \frac{4}{3}i,$ $\xi_{01} = \xi_{02} = \xi_{03} = \xi_{04} = 0,$ $\gamma_1 = \gamma_2 = 1, \gamma_3 = \gamma_4 = \gamma_5 = -1$
	The period and kink period solitons (II)	$k_1 = k_2 = \frac{3}{4},\ s_1 = \frac{6}{5}i,\ s_2 = -\frac{6}{5}i,\ k_3 = k_4 = \frac{2}{3},\ s_3 = 1 - \frac{4}{3}i,\ s_4 = 1 + \frac{4}{3}i,$ $\xi_{01} = \xi_{02} = \xi_{03} = \xi_{04} = 0,$ $\gamma_1 = \gamma_2 = 1, \gamma_3 = \gamma_4 = \gamma_5 = -1$
	Multi-lump solitons	$k_1 = k_2 = 0.01,\ s_1 = s_2^* = 0.01 + 0.01i,\ k_3 = k_4 = 0.02,\ s_3 = s_4^* = 0.02 + 0.02i,\ s_4 = 1 + \frac{4}{3}i,$ $\xi_{01} = \xi_{02} = \xi_{03} = \xi_{04} = i\pi,$ $\gamma_1 = \gamma_2 = -1, \gamma_3 = \gamma_4 = \gamma_5 = 1$

3 Conclusion

This study is based on the application of the Hirota bilinear method to systematically investigate the (2+1)-dimensional generalized Bogoyavlensky-Konopelchenko-equation and have obtained a series of analytical solutions ranging from one to four soliton solutions. By ingeniously setting the parameter relationship, we found that the higher-order soliton solutions of this equation can degenerate into various rich local wave interaction patterns. Specifically, when the parameters are real numbers, the system presents the basic line soliton and kink soliton. By imposing certain parameter constraints, second-order soliton solution can produce periodic and kink periodic solitons. For the third soliton solutions, we have observed the interaction between periodic soliton and line soliton (or kink soliton). For the four soliton solutions, we have further obtained complex interaction patterns such as two-periodic solitons or two-line solitons and a periodic soliton. Furthermore, by using the long-wave limit method, we have successfully constructed lump soliton, line soliton, lump soliton composite structures and multi-lump soliton solutions. To reveal the dynamic behaviors of these solitons, we have shown the corresponding three-dimensional diagrams and density diagrams by means of Maple software. Tables 1-3 systematically summarize the correspondence between parameter selections and the respective soliton interaction patterns, offering a theoretical guide for controlling and modulating nonlinear waves. Although this research uncovered a variety of rich localized wave interaction phenomena, further exploration is still needed to understand more nonlinear wave patterns and more interesting complex interaction mechanisms underlying in this model. The obtained results demonstrate the powerful capability (Osman & Machado, 2018) and superiority of Hirota bilinear method in dealing with higher-dimensional integrable systems and constructing soliton solutions. These findings hold significant theoretical importance for understanding the internal mechanisms of energy localization and wave propagation processes in nonlinear physics.

References

Ablowitz, M. J., Kaup, D. J., Newell, A. C., & Segur, H. (1974). The inverse scattering transform-Fourier analysis for nonlinear problems. Studies in applied mathematics, 53(4), 249-315.

Ai, L., & Xu, J. (2019). On a Riemann–Hilbert problem for the Fokas–Lenells equation. Applied Mathematics Letters, 87, 57-63.

Akram, S., Ahmad, J., Rehman, S. U., & Ali, A. (2023). New family of solitary wave solutions to new generalized Bogoyavlensky–Konopelchenko equation in fluid mechanics. International Journal of Applied and Computational Mathematics, 9(5), 63.

An, Y. N., & Guo, R. (2023). The mixed solutions of the (2+ 1)-dimensional Hirota–Satsuma–Ito equation and the analysis of nonlinear transformed waves. Nonlinear Dynamics, 111(19), 18291-18311.

Bilman, D., & Miller, P. D. (2019). A robust inverse scattering transform for the focusing nonlinear Schrödinger equation. Communications on Pure and Applied Mathematics, 72(8), 1722-1805.

Biswas, S., Ghosh, U., & Raut, S. (2023). Construction of fractional granular model and bright, dark, lump, breather types soliton solutions using Hirota bilinear method. Chaos, Solitons & Fractals, 172, 113520.

Chen, S. T., & Ma, W. X. (2018). Lump solutions to a generalized Bogoyavlensky-Konopelchenko equation. Frontiers of Mathematics in China, 13(3), 525-534.

Chen, Y., & Yan, X. W. (2022). Inverse scattering and soliton solutions of high-order matrix nonlinear Schrödinger equation. Nonlinear Dynamics, 108(4), 4057-4067.

Clarkson, P. A., & Kruskal, M. D. (1989). New similarity reductions of the Boussinesq equation. Journal of Mathematical Physics, 30(10), 2201-2213.

Faisal, K., & Maqbool, K. (2025). New soliton solutions of (2+ 1)-dimensional Bogoyavlensky-Konopelchenko equation via two integration techniques. Applied Mathematics-A Journal of Chinese Universities, 40(1), 169-181.

Fang, T., & Wang, Y. H. (2018). Interaction solutions for a dimensionally reduced Hirota bilinear equation. Computers & Mathematics with Applications, 76(6), 1476-1485.

Fokas, A. S., & Kapaev, A. A. (2000). A Riemann–Hilbert approach to the Laplace equation. Journal of mathematical analysis and applications, 251(2), 770-804.

Freeman, N. C., & Nimmo, J. J. C. (1983). Soliton solutions of the Korteweg de Vries and the Kadomtsev-Petviashvili equations: the Wronskian technique. Proceedings of the Royal Society of London. A. Mathematical and Physical Sciences, 389(1797), 319-329.

Gao, L. N., Zhao, X. Y., Zi, Y. Y., Yu, J., & Lü, X. (2016). Resonant behavior of multiple wave solutions to a Hirota bilinear equation. Computers & Mathematics with Applications, 72(5), 1225-1229.

Gardner, C. S., Greene, J. M., Kruskal, M. D., & Miura, R. M. (1967). Method for solving the Korteweg-deVries equation. Physical review letters, 19(19), 1095.

Geng, X., & Tam, H. W. (1999). Darboux transformation and soliton solutions for generalized nonlinear Schrödinger equations. Journal of the Physical Society of Japan, 68(5), 1508-1512.

Gorshkov, K. A., & Ostrovsky, L. A. (1981). Interactions of solitons in nonintegrable systems: direct perturbation method and applications. Physica D: Nonlinear Phenomena, 3(1-2), 428-438.

Grammaticos, B., Ramani, A., & Hietarinta, J. (1994). Multilinear operators: the natural extension of Hirota's bilinear formalism. Physics Letters A, 190(1), 65-70.

Han, Y., Zhuang, J., & Liu, Y. (2025). Neural network-enhanced bilinear framework for analytical soliton dynamics and wave interactions in (3+ 1)-dimensional Hirota–Satsuma–Ito system. The European Physical Journal Special Topics, 234(18), 5561-5581.

Hietarinta, J. (1987). A search for bilinear equations passing Hirota's three-soliton condition. I. KdV-type bilinear equations. Journal of Mathematical Physics, 28(8), 1732-1742.

Hietarinta, J. (1996). Gauge symmetry and the generalization of Hirota's bilinear method. Journal of Nonlinear Mathematical Physics, 3(3-4), 260-265.

Hirota, R. (1974). A new form of Bäcklund transformations and its relation to the inverse scattering problem. Progress of Theoretical Physics, 52(5), 1498-1512.

Hirota, R. (1989). Soliton solutions to the BKP equations. I. The Pfaffian technique. Journal of the Physical Society of Japan, 58(7), 2285-2296.

Hirota, R., & Satsuma, J. (1977). Nonlinear evolution equations generated from the Bäcklund transformation for the Boussinesq equation. Progress of Theoretical Physics, 57(3), 797-807.

Hua, Y. F., Guo, B. L., Ma, W. X., & Lü, X. (2019). Interaction behavior associated with a generalized (2+ 1)-dimensional Hirota bilinear equation for nonlinear waves. Applied Mathematical Modelling, 74, 184-198.

Johansson, M., & Aubry, S. (1997). Existence and stability of quasiperiodic breathers in the discrete nonlinear Schrödinger equation. Nonlinearity, 10(5), 1151.

Li, Y., Tian, S. F., & Yang, J. J. (2022). Riemann–Hilbert problem and interactions of solitons in the-component nonlinear Schrödinger equations. Studies in Applied Mathematics, 148(2), 577-605.

Li, Y., Yao, R., & Lou, S. (2023). An extended Hirota bilinear method and new wave structures of (2+ 1)-dimensional Sawada–Kotera equation. Applied Mathematics Letters, 145, 108760.

Ling, L., Zhao, L. C., & Guo, B. (2015). Darboux transformation and multi-dark soliton for N-component nonlinear Schrödinger equations. Nonlinearity, 28(9), 3243-3261.

Liu, Y., Wen, X. Y., & Wang, D. S. (2019). The N-soliton solution and localized wave interaction solutions of the (2+ 1)-dimensional generalized Hirota-Satsuma-Ito equation. Computers & Mathematics with Applications, 77(4), 947-966.

Lou, S. Y., Tang, X. Y., & Lin, J. (2000). Similarity and conditional similarity reductions of a (2+ 1)-dimensional KdV equation via a direct method. Journal of Mathematical Physics, 41(12), 8286-8303.

Lu, X., Lin, F., & Qi, F. (2015). Analytical study on a two-dimensional Korteweg-de Vries model with bilinear representation, Backlund transformation and soliton solutions. Applied Mathematical Modelling, 39(12), 3221-3226.

Lü, X., Zhu, H. W., Meng, X. H., Yang, Z. C., & Tian, B. (2007). Soliton solutions and a Bäcklund transformation for a generalized nonlinear Schrödinger equation with variable coefficients from optical fiber communications. Journal of Mathematical Analysis and Applications, 336(2), 1305-1315.

Ludlow, D. K., Clarkson, P. A., & Bassom, A. P. (1999). Similarity reductions and exact solutions for the two-dimensional incompressible Navier–Stokes equations. Studies in Applied Mathematics, 103(3), 183-240.

Lv, N., Li, J., Yuan, X., & Wang, R. (2023). Controllable rogue waves in a compressible hyperelastic plate. Physics Letters A, 461, 128639.

Ma, W. X. (2004). Wronskians, generalized Wronskians and solutions to the Korteweg–de Vries equation. Chaos, Solitons & Fractals, 19(1), 163-170.

Ma, W. X. (2022). Soliton solutions by means of Hirota bilinear forms. Partial Differential Equations in Applied Mathematics, 5, 100220.

Ma, W. X., Zhang, Y., Tang, Y., & Tu, J. (2012). Hirota bilinear equations with linear subspaces of solutions. Applied Mathematics and Computation, 218(13), 7174-7183.

Ma, W. X., Zhang, Y., Tang, Y., & Tu, J. (2012). Hirota bilinear equations with linear subspaces of solutions. Applied Mathematics and Computation, 218(13), 7174-7183.

Mabrouk, S. M., & Rashed, A. S. (2019). N-Solitons, kink and periodic wave solutions for (3+ 1)-dimensional Hirota bilinear equation using three distinct techniques. Chinese Journal of Physics, 60, 48-60.

Manafian, J., Mohammadi Ivatloo, B., & Abapour, M. (2020). Breather wave, periodic, and cross-kink solutions to the generalized Bogoyavlensky-Konopelchenko equation. Mathematical Methods in the Applied Sciences, 43(4), 1753-1774.

Mandal, U. K., Malik, S., Kumar, S., & Das, A. (2023). A generalized (2+ 1)-dimensional Hirota bilinear equation: integrability, solitons and invariant solutions. Nonlinear Dynamics, 111(5), 4593-4611.

Osman, M. S., & Machado, J. A. T. (2018). The dynamical behavior of mixed-type soliton solutions described by (2+ 1)-dimensional Bogoyavlensky–Konopelchenko equation with variable coefficients. Journal of Electromagnetic Waves and Applications, 32(11), 1457-1464.

Pashaev, O., & Tanoğlu, G. (2005). Vector shock soliton and the Hirota bilinear method. Chaos, Solitons & Fractals, 26(1), 95-105.

Ray, S. S. (2017). On conservation laws by Lie symmetry analysis for (2+ 1)-dimensional Bogoyavlensky–Konopelchenko equation in wave propagation. Computers & Mathematics with Applications, 74(6), 1158-1165.

Razzaq, W., & Zafar, A. (2025). Bilinearization of generalized Bogoyavlensky-Konopelchenko equation for Solitons with Neural Network: Painleve analysis: W. Razzaq, A. Zafar. Nonlinear Dynamics, 1-14.

Saifullah, S., Ahmad, S., Alyami, M. A., & Inc, M. (2022). Analysis of interaction of lump solutions with kink-soliton solutions of the generalized perturbed KdV equation using Hirota-bilinear approach. Physics Letters A, 454, 128503.

Shepelsky, D., & Zielinski, L. (2017). The inverse scattering transform in the form of a Riemann-Hilbert problem for the Dullin-Gottwald-Holm equation. Opuscula Mathematica, 37(1), 167-187.

Tchokouansi, H. T., Kuetche, V. K., & Kofane, T. C. (2016). On the propagation of solitons in ferrites: The inverse scattering approach. Chaos, Solitons & Fractals, 86, 64-74.

Triki, H., Jovanoski, Z., & Biswas, A. (2014). Shock wave solutions to the Bogoyavlensky–Konopelchenko equation. Indian Journal of Physics, 88(1), 71-74.

Ünal, M. (2010). Application of the Pfaffian technique to the KR and mNVN equations. Journal of mathematical analysis and applications, 362(1), 224-230.

Wahlquist, H. D., & Estabrook, F. B. (1973). Bäcklund transformation for solutions of the Korteweg-de Vries equation. Physical review letters, 31(23), 1386.

Wang, S. (2023). Novel soliton solutions of CNLSEs with Hirota bilinear method. Journal of Optics, 52(3), 1602-1607.

Wang, X., & Wei, J. (2022). Three types of Darboux transformation and general soliton solutions for the space-shifted nonlocal PT symmetric nonlinear Schrödinger equation. Applied Mathematics Letters, 130, 107998.

Wu, X. H., & Gao, Y. T. (2023). Generalized Darboux transformation and solitons for the Ablowitz–Ladik equation in an electrical lattice. Applied Mathematics Letters, 137, 108476.

Xia, B., Zhou, R., & Qiao, Z. (2016). Darboux transformation and multi-soliton solutions of the Camassa-Holm equation and modified Camassa-Holm equation. Journal of Mathematical Physics, 57(10).

Yokuş, A., Duran, S., & Kaya, D. (2024). An expansion method for generating travelling wave solutions for the (2+ 1)-dimensional Bogoyavlensky-Konopelchenko equation with variable coefficients. Chaos, Solitons & Fractals, 178, 114316.

Zuo, J. M., & Zhang, Y. M. (2011). The Hirota bilinear method for the coupled Burgers equation and the high-order Boussinesq—Burgers equation. Chinese Physics B, 20(1), 010205.

Zou, Z., & Guo, R. (2023). The Riemann–Hilbert approach for the higher-order Gerdjikov–Ivanov equation, soliton interactions and position shift. Communications in Nonlinear Science and Numerical Simulation, 124, 107316.